

**Fabrication and Photocatalytic Properties of Carbon
nanotube/C₆₀ Heterojunction Decorated with TiO_x**

September, 2017

Kiki Kurniawan

77426551

Graduate School of Environmental and Life Science

(Doctor Course)

OKAYAMA UNIVERSITY

Contents

Chapter 1 General Introduction	1
1.1 Semiconductor materials acting as photocatalysts	2
1.2 Issue on solar-light driven photocatalyst	4
1.3 Advantage of single-walled carbon nanotubes (SWCNTs) for a solar-light absorber	5
1.4 Issues on making s-SWCNT-photocatalysts	8
1.5 s-SWCNTs/C ₆₀ heterojunction for solar cells	13
2. Fullerodendron	14
2.1 C ₆₀ moiety can associate with CNTs through π - π interaction.	15
2.2 PAMAM dendron unit of fullerodendron shows the affinity to inorganic materials.	16
3. Photosensitized hydrogen evolution from water using SWCNTs/C ₆₀ coaxial composites	19
4. Why we introduce TiO _x layer into the shell of the SWCNT-photocatalyst	21
4.1 Transition metal oxide	21
4.1 Electron-extraction layer attained with a combination of C ₆₀ layer	23
4.2 Hole blocking layer for organic solar cells	24
5. Purpose of this work	25
References	27
Chapter 2 Effect of TiO_x shell on photocatalytic activity of the SWCNT-photocatalyst	31
2.1 Introduction	32
2.2 Experimental Section	34

2.2.1 General	34
2.2.2 Preparation of SWCNT/fullerodendron supramolecular nanocomposites	35
2.2.3 Fabrication of SWCNT/fullerodendron/TiO _x coaxial nano-hybrids	35
2.2.4 Synthesis of colloidal PVP-Pt	36
2.2.5 Hydrogen evolution	36
2.2 Preparation SWCNTs solution for spray coating	37
2.3.1 Preparation thin film SWCNTs	37
2.3.2 Decoration thin film SWCNT with fullrodendron	38
2.3.3 Decoration TiO _x on the surface of thin film SWCNT/fullerodendron	38
2.4 Results and discussion	39
2.4.1 Fabrication of SWCNT/fullerodendron/TiO _x	39
2.4.2 Characterization of SWCNT/fullerodendron/TiO _x	39
2.4.3 Application of SWCNT/fullerodendron/TiO _x coaxial nano-hybrids	46
2.5 Energy-level diagram of the SWCNT/fullerodendron/TiO _x	48
2.6 Fabrication Thin Film FTO/SWCNT/fullerodendron/TiO _x	49
2.6.1 Hydrogen Evolution from Thin Film SWCNT/fullerodendron/TiO _x	50
2.6.2 Photoelectrode Hydrogen Evolution	51
2.7 Summary	51
References	53
Chapter 3. Conclusion	56
Acknowledgement	60
List of Publications	61

Chapter 1

General Introduction

1.1 Semiconductor Materials Acting as Photocatalysts

The Sun, which locates at the center of solar system, supports nearly all the life on earth by irradiating solar light. For example, through the well-known photosynthesis process, plants and other organisms can convert the solar light energy to chemical energy (such as carbohydrate molecules).¹ In other words, all of the organic compounds and most of the energy, which are necessary for life on earth, are originated from the photosynthesis. Nearly all the forms of energy (coal, oil, natural gas, etc.) are from solar energy. These abundant and economical energies greatly promoted the civilization of human. However, after the industrial revolution, energy consumption was rapidly increased with the improvement of living standards and gave rise to the energy crisis. Meantime, environmental pollution and global warming have been also the main problems in need of extrications for the sustainable development of our society.

Displacement of the traditional energy, such as fossil fuels, by the renewable and clean solar energy is necessary to solve the global problems. One important and potential technology relating to this concept is conversions of abundant natural resources into the fuels using solar energy through photocatalysis. Especially hydrogen production by the use of photocatalytic water splitting relieves the problem of the energy crisis and global warming.² In this context, various photocatalytic systems exhibiting moderate solar energy conversion efficiencies have been developed so far. Especially, inorganic semiconductor materials are well explored because of their photocatalytic activities under solar light.³ The photocatalytic

reaction takes place on the surface of the photocatalysts, where the redox reaction occurs to produce, for instance, hydrogen. Owing to the excitation of semiconducting photocatalysts with light-wavelength equal to or greater than their band gap energies, mobile holes and electrons can be generated in valence and conduction bands, respectively. Figure 1-1 illustrates the band gap energies of several semiconductors in aqueous electrolyte.⁴

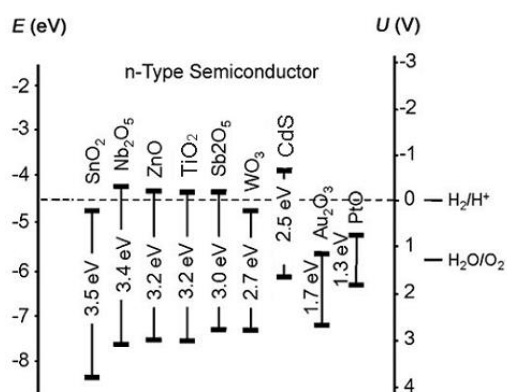


Figure 1-1. Band energy levels and band gap energies of semiconductors used as photocatalysts corresponding energy scales vs. the vacuum level (eV) and vs. the normal hydrogen electrode (NHE) (V).

Then electrons and holes can facilitate the redox reactions in the photocatalytic process (Figure 1-2). It is notable that the absorption of the photocatalysts corresponds to their band gap energies.⁵

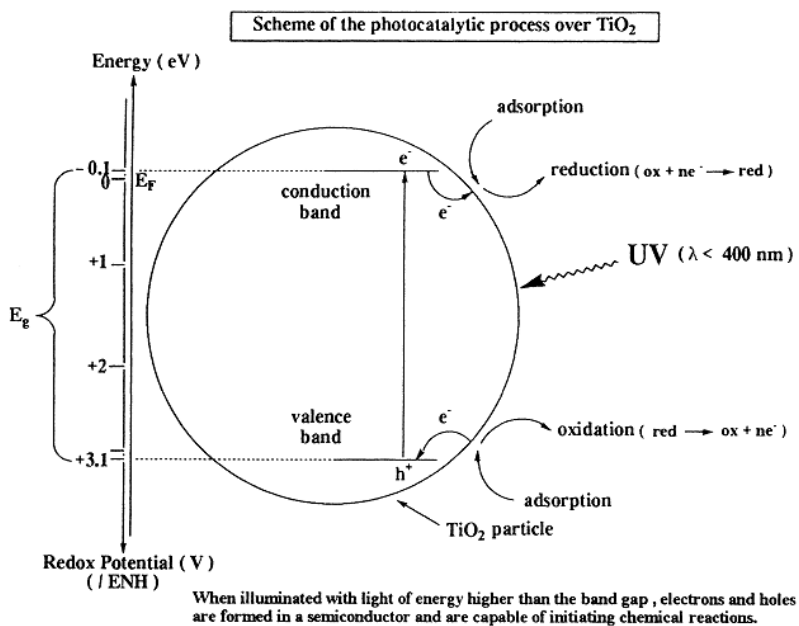


Figure 1-2. Energy band diagram of a spherical titania particle.

1.2 Issue on Solar-Light Driven Photocatalyst

From the viewpoint of an effective use of the sun-light, the photocatalytic activity in long wavelength region ($> 600 \text{ nm}$) is a problem of the ordinal inorganic photocatalysts. Because the energetic ratio occupied by the wavelength shorter than 600 nm is only about 30% among the solar spectrum. In this context, Domen reported phthalocyanine dye sensitization of mpg-C₃N₄ photocatalyst for H₂ evolution, in an attempt to absorb 660-nm-light (Figure 1-3).⁶

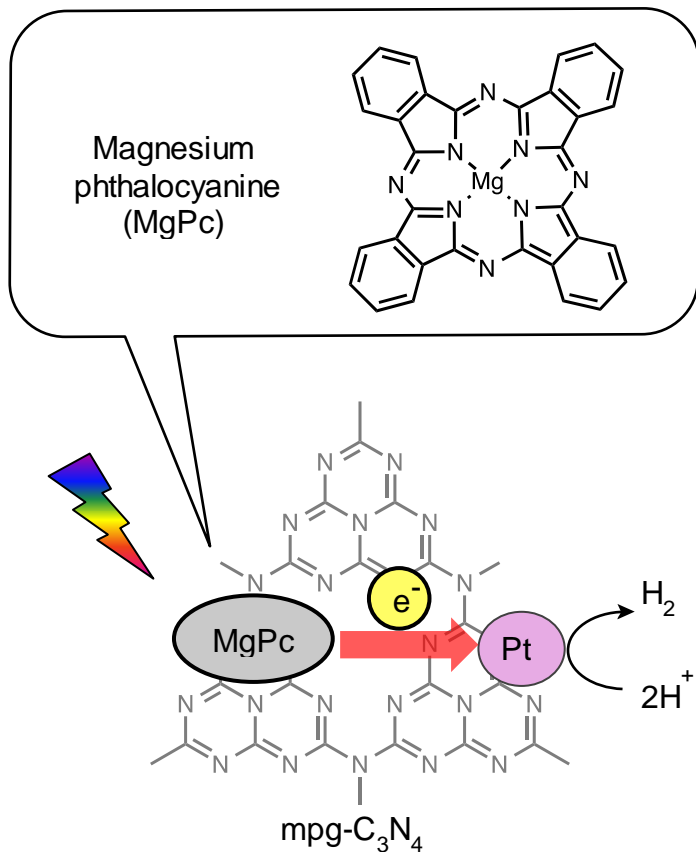


Figure 1-3. Hydrogen generating photocatalyst having activity in long wavelength region.

1.3 Advantage of Single-walled Carbon Nanotubes (SWCNTs) for a Solar-Light Absorber

A single-wall carbon nanotube (SWCNT) is a hollow cylinder formed by rolling up a graphene sheet along a chiral vector (Figure 1-4).⁷ The circumference of the SWCNT is determined by a chiral vector, $C_h = n a_1 + m a_2$, where (n, m) are integers known as the chiral indices and a_1 and a_2 are the unit vectors of the graphene lattice. The structures of SWCNTs

strongly affect their electrical and optical properties. Depending on these chiral angles and diameters, SWCNTs show semiconducting (s-SWCNT) or metallic (m-SWCNT) in nature. In particular, their band gaps can vary from zero to about 2 eV and electrical conductivity can be in a range of a metal or semiconductor. For a given (n, m) nanotube, when $n = m$, the nanotube is metallic; when $n-m$ is a multiple of 3, the SWCNTs are semiconducting with geometry-dependent band gaps.

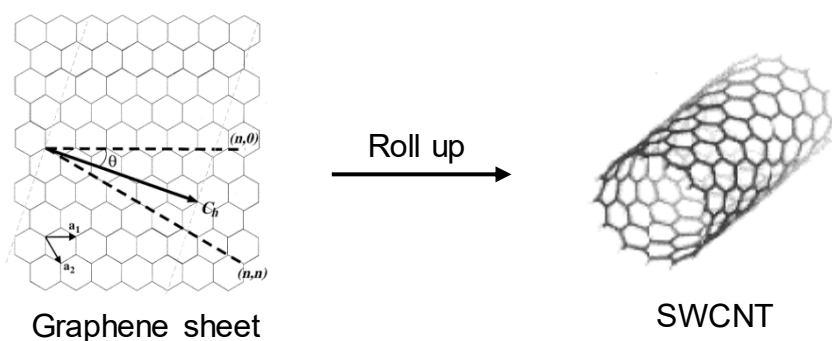


Figure 1-4. Schematic of a portion of a graphene sheet rolled up to form a SWCNTs.

In general, as-synthesized SWCNTs are composed of s-SWCNTs and m-SWCNTs in an approximately 2:1 ratio.^{8,9,10} Arnold reported in m-SWCNTs, there is a finite (one-dimensional density of states) (DOS) in between the lowest conduction and valence VHS (Van Hove Singularities) (VHS), and the lowest-energy ground-state electrons reside at the Fermi energy in the middle of the gap. In contrast, s-SWCNTs have no DOS in between the lowest-energy conduction and valence VHS, and the lowest-energy electrons (in undoped-SWCNTs) reside at the top of the valence VHS (Figure 1-5).¹¹

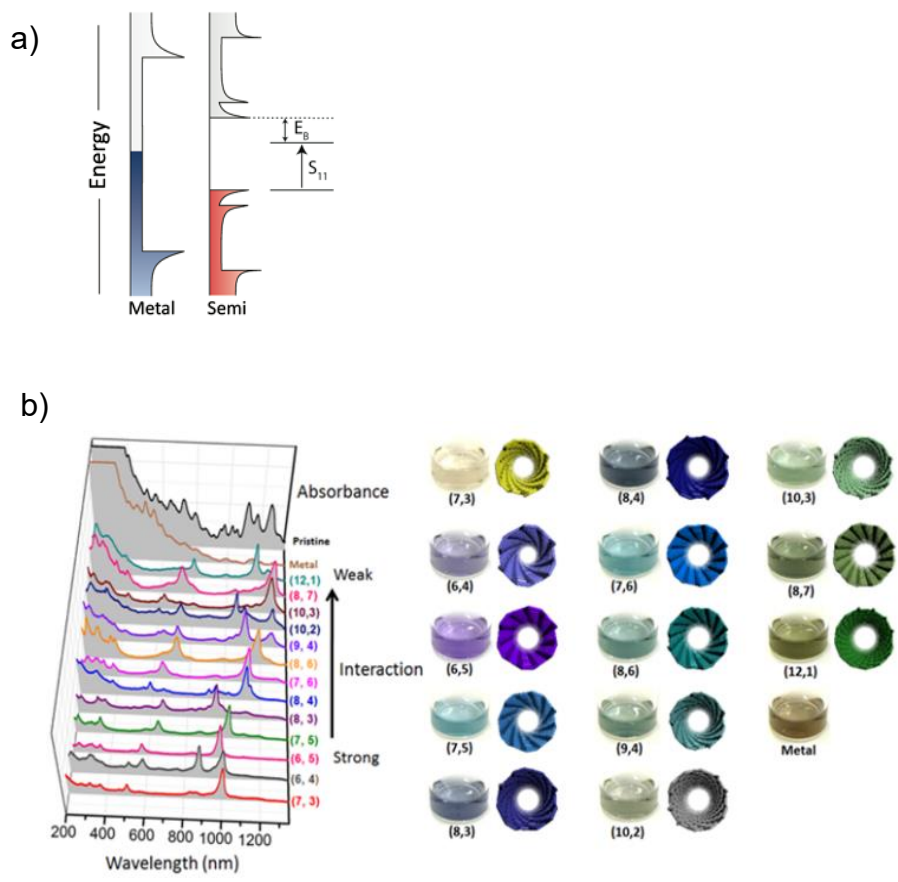


Figure 1-5. a) Single-particle DOS for m-SWCNTs (left) and s-SWCNTs (right). b) Various kind of s-SWCNTs.¹²

The bandgap and optical properties of s-SWCNTs are widely tunable with the chirality of s-SWCNT, enabling either the selective or broadband absorption of light spanning from the ultraviolet to the near-infrared.¹³ This strong point makes s-SWCNTs quite promising for solar energy harvesting. For example, the solar energy conversion efficiency of the solar cell based on (6,5) SWCNT is predicted to be ca. 7% (Figure 1-6).⁹

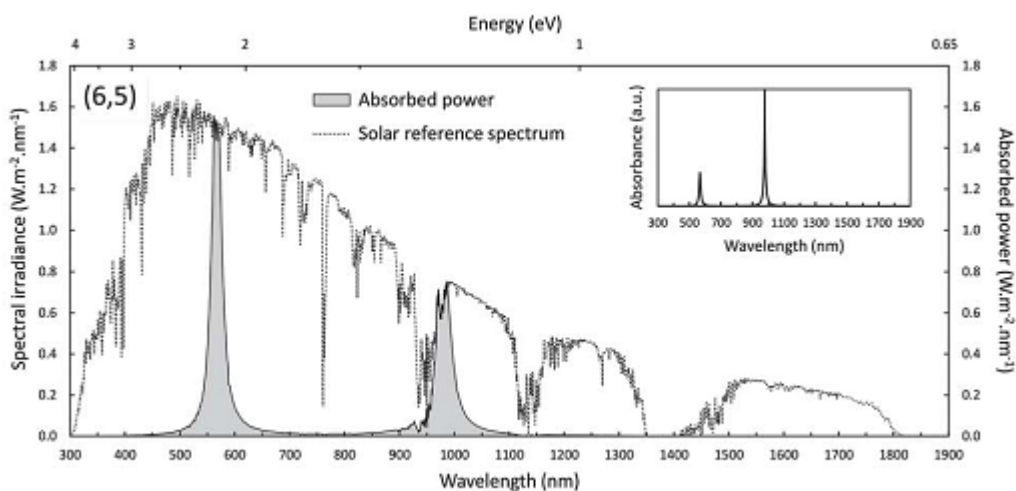


Figure 1-6. Absorption for the solar cell consisting of (6,5)SWCNT overlaid with the solar spectrum.

1.4 Issues on Making s-SWCNT-Photocatalysts

a) Poor Solubility of SWCNTs

s-SWCNTs are insoluble in aqueous or organic solvents, owing to their extremely strong van der Waals interaction (Figure 1-7).¹⁴ Since the lateral surface could act as the reaction sites of photocatalytic reactions, isolation of the individual s-SWCNTs via through a debundling process in the reaction media is required. Furthermore, the bundles composed of the mixture of various chiralities are not appropriate to use for photovoltaics and photocatalysts because of an energy migration between s-SWCNTs and trapping of mobile carriers. However, there is no good example of a dispersant of s-SWCNT to produce SWCNT-photocatalyst, although several reports described the solar cell fabrication through a physical modification of s-SWCNTs using π - π interaction.¹⁵



Figure 1-7. Van Der Wall interaction between SWCNTs leads to the formation of a bundle.

b) Large Binding Energy of Electron-hole Pairs (exciton).

Typically, bundled SWCNTs do not exhibit fluorescence because of the quenching of the excited state due to m-SWCNTs or thermal quenching. Then isolation of s-SWCNTs is necessary to use the photoexcited state of s-SWCNTs. However, even the photoexcitation of isolated s-SWCNTs does not generate a hole (h^+) and an electron (e^-) because of large binding energy of an exciton (an electron-hole pair). To observe the dissociation of the exciton, Fleming and colleagues used a pulse pumping laser to generate higher exciton state via exciton-exciton annihilations (Figure 1-8).¹⁶ An exciton binding energy of 0.41 eV is determined experimentally for a selected nanotube type, the (8,3) tube, from the estimation of the energy difference between an electron-hole continuum and its precursor exciton.

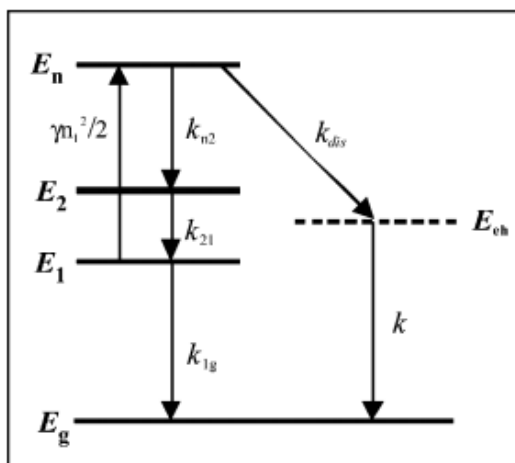


Figure 1-8. Schematic description of the electronic structure of the (8,3)tube and the exciton relaxation pathways.

Dukovic and colleagues also determined the exciton binding energies by the use of two-photon excitation spectroscopy.¹⁷ Figure 1-9 represents schematic representation of electronic transitions associated with the band gap in semiconducting SWNTs. The states below the band gap are bound excitons. One-photon absorption is allowed for the lowest-lying $1u$ state, while two-photon absorption is allowed for the $2g$ state. Absorption of two photons by the $2g$ and continuum states is followed by emission from the $1u$ state. Notably, exciton binding energies are large and vary inversely with nanotube diameter. The exciton binding energies were estimated to be 0.42 eV for (8,3)tube and 0.27 eV for (11,7)tube, respectively, which consisted with the determination reported by Fleming.¹⁶

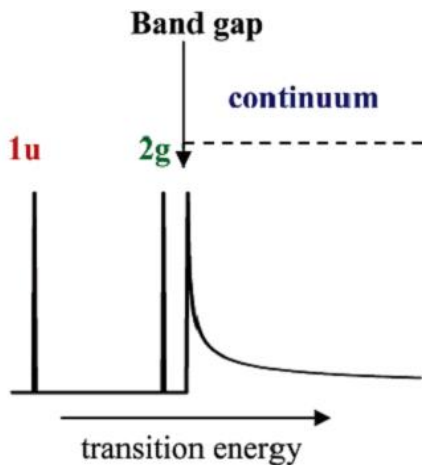


Figure 1-9. Schematic representation of electronic transitions associated with the band gap in semiconducting SWCNTs.

Wang et. al. also reported the binding energy of exciton, ca. 400 meV for s-SWCNT with 0.8-nanometer diameters, estimated by the two-photon excitation spectroscopy (Figure 1-10).¹⁸ The measured fluorescence intensity is shown in a false-color representation as a function of the (two-photon) excitation energy and the (one-photon) fluorescence emission energy. Fluorescence peaks of (7,5), (6,5), (8,3), and (9,1) tubes (aligned with increasing emission energy) can be identified by black circles. The two-photon excitation peaks are shifted substantially above the energy of the corresponding emission feature, as is apparent by comparison with the solid line describing equal excitation and emission energies. The large shift arises from the excitonic nature of SWCNTs optical transitions.

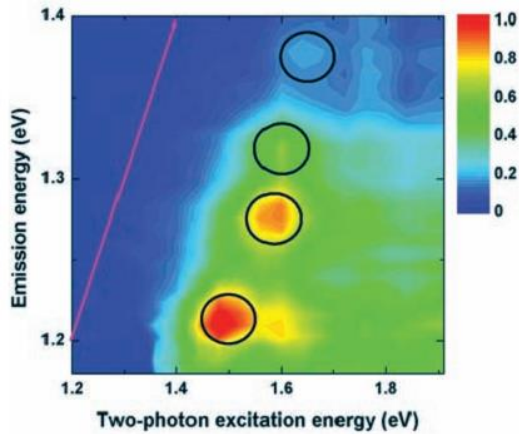


Figure 1-10. Contour plot of two-photon excitation spectra of SWCNTs.

Figure 1-11(a) shows a schematic picture of one-photon absorption and emission in carbon nanotubes. E_{11} indicates the single-particle transition between the lowest sub bands. Emission occurs from the lowest one-photon active $1u$ state. Figure 1-11(b) shows two-photon absorption results in the excitation of exciton states. The luminescence of s-SWCNT for excitation below the band gap between 1210 and 1970 nm is shown in Figure 1-11(c). Combining this experiment and theory, Maultzsch and co-workers determined binding energies of 0.3–0.4 eV for nanotubes with diameters between 6.8 and 9.0 Å.¹⁹

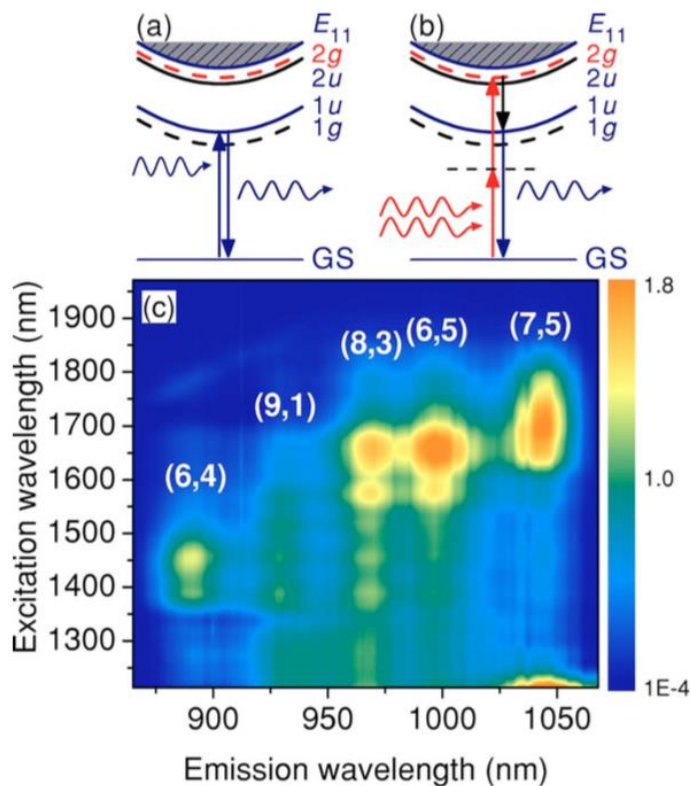


Figure 1-11. (a) Schematic picture of one-photon absorption and emission in carbon nanotubes. (b) Two-photon absorption and emission in carbon nanotubes. (c) Two-photon luminescence spectra of carbon nanotubes.

1.5 s-SWCNTs/ C_{60} Heterojunction for Solar Cells

Recently, construction of heterojunction between s-SWCNT and electron acceptors have been attracted a great attention in order to generate an electron (e^-) and a hole (h^+) from the exciton in s-SWCNTs. In particular, since C_{60} can provide an appropriate band offset (~ 130 meV), there is an increasing focus on s-SWCNT/ C_{60} heterojunction. Although Takaguchi and colleagues reported the first example of a water-dispersible

SWCNT nanocomposite having an ideal coaxial SWCNT/C₆₀ heterojunction,²⁰ its application for photovoltaic devices was behind in other simple mixture of SWCNTs and C₆₀. Imahori et. al. reported dye-sensitized solar cells by the use of SWCNT/C₆₀ and SWCNT/C₇₀ composites as dye moieties.^{14,21} Arnold et. al. reported a photovoltaic film device made by deposition of the C₆₀ film on the s-SWCNT film, where the dissociation of exciton into h⁺ and e⁻ at the interface between two films (Figure 1-12).²²

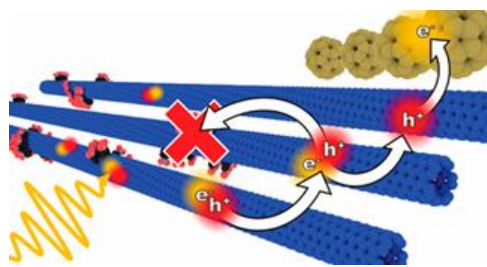


Figure 1-12. Exciton dissociation at SWCNT/C₆₀ heterojunction.

2. Fulleredendron

Fullerene-functionalized dendrimers, i.e., fulleredendrimer, are attractive candidates for a variety of interesting features in supramolecular chemistry and materials science.^{24,25,26} Takaguchi reported the synthesis of water-soluble fulleredendron by a Diels-Alder reaction of C₆₀ with poly(amidoamine) (PAMAM) dendron bearing an anthracene moiety at the focal point.^{27,28} There are two advantages of the fulleredendron for construction of nanocarbon nanohybrids (Figure 1-13):

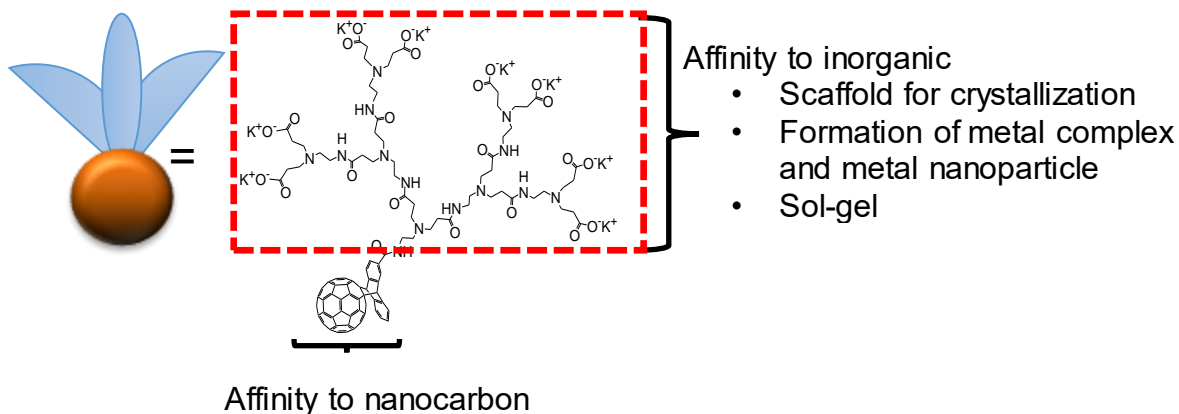


Figure 1-13. Advantages of fullerodendron for construction of nanocarbon hybrids.

2.1 “C₆₀ moiety can associate with CNTs through π - π interaction.”

Imahori and coworkers reported the formation of SWCNT/C₆₀ and SWCNT/C₇₀ (Figure 1-14a).^{14,21} A C₆₀ unit of fullerodendron also can associate with SWCNTs. Takaguchi have reported that fullerodendron was very effective at dispersing SWCNTs in water via the formation of supramolecular nanocomposites, although SWCNT/C₆₀ reported by Imahori’s group is not dispersible in any solvents (Figure 1-14b).²⁹

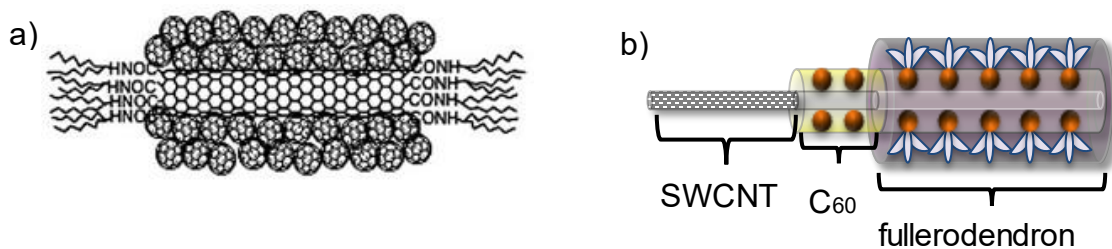


Figure 1-14. a) SWCNTs/C₆₀ composites and b) SWCNTs/fullerodendron.

2.2 “PAMAM dendron unit of fullerodendron shows the affinity to inorganic materials.”

Three examples of the fabrication of the hybrids consisting of fullerodendron and inorganic materials are described as follows;

(a) Scaffold for the crystallization of inorganic materials in solution system

It is well-known that PAMAM dendrimer is useful for the nucleation site of crystallization.^{20,30-33} Takaguchi et al. reported the fabrication of C₆₀/CaCO₃ composites,³⁴ and SWCNT/CaCO₃ hybrids³⁵ by the use of fullerodendron through the biomimetic crystallization process. Furthermore, MWCNT/CaCO₃ and MWCNT/CaCl₂ nanohybrids were fabricated by the use of PAMAM dendrimer having a 1,10-bis(decyloxy)decane core.³⁶ The dendritic dispersants act as an effective ‘glue’ between the CNTs and inorganic crystals and enable the facile formation of CNT/inorganic hybrids (Figure 1-15).

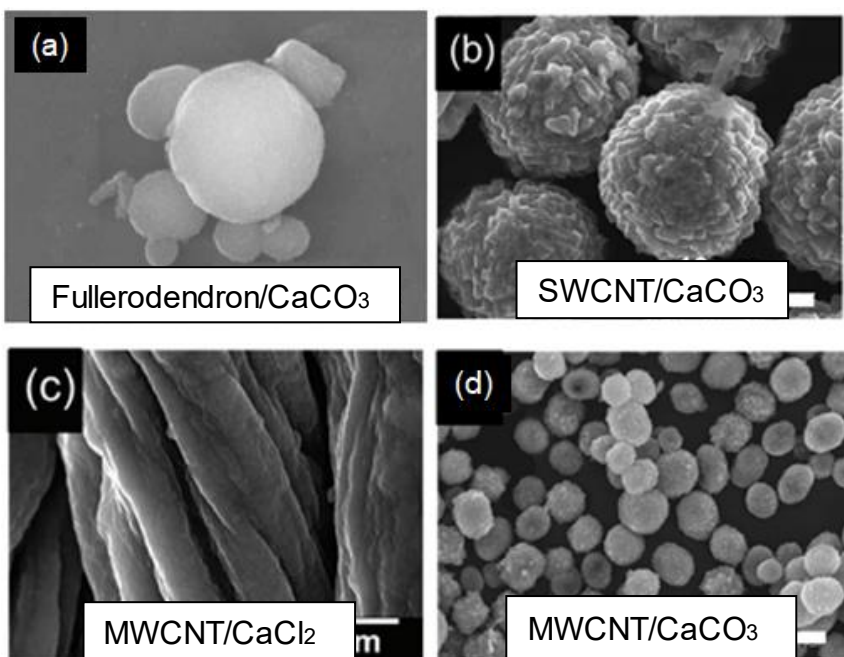


Figure 1-15. SEM images of nanocarbon/ CaCO_3 hybrids obtained by the biomimetic crystallization process using dendritic ‘glue’ molecules.

(b) Coordination sites for metal complex and stabilizer of metal nanoparticle

PAMAM dendrimer has many metal-ion-coordination sites, such as tertiary amine groups and CO^{2-} . Therefore, PAMAM dendrimer itself act as ligand of metal ion.³⁷ In addition, subsequent reduction of the complex with NaBH_4 affords encapsulated zero-valent metal nanoparticles (Figure 1-16). Takaguchi et. al. reported the direct incorporation of Pt(II) into the shell of SWCNT/fullerodendron supramolecular nanocomposites (Figure 1-17).^{38,39}

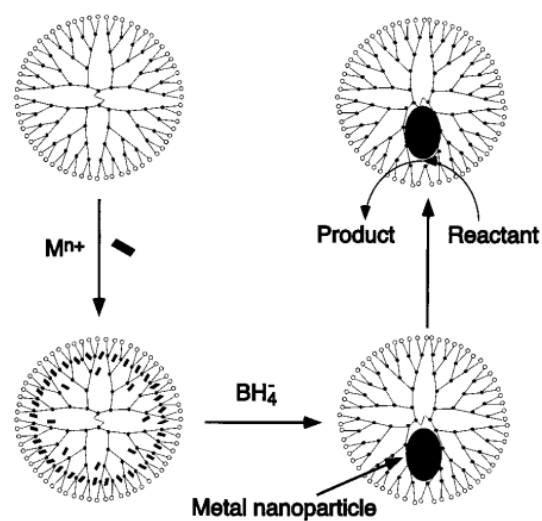


Figure 1-16. PAMAM dendrimer metal complex and PAMAM dendrimer encapsulated metal nanoparticle.

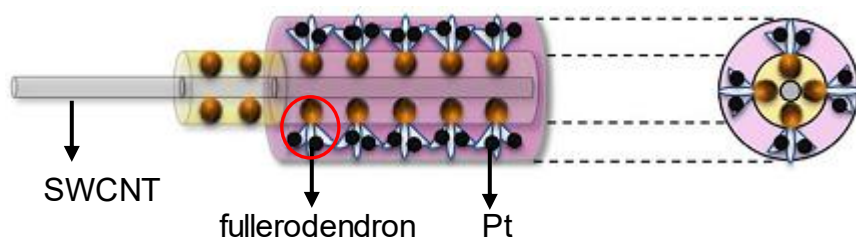


Figure 1-17. Schematic illustration of SWCNT/fullerodendron/Pt(II) coaxial nano-hybrids.

(c) Catalyst of sol-gel condensation

Takaguchi et. al. reported the SWCNT/fullerodendron/SiO₂ coaxial nanohybrid, which was fabricated by sol-gel polycondensation of tetraethoxysilane (TEOS) on the surface of SWCNT/fullerodendron supramolecular nanocomposite (Figure 1-18).⁴⁰

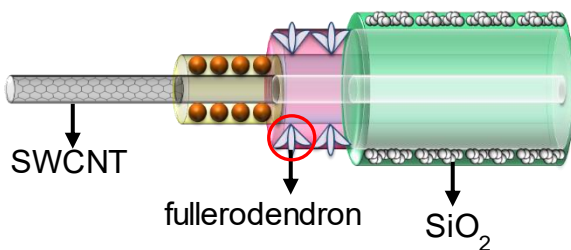


Figure 1-18. Schematic illustration of SWCNT/fullerodendron/SiO₂ coaxial nano-hybrids.

3. Photosensitized Hydrogen Evolution from Water Using SWCNTs/C₆₀ Coaxial Composites

Recent theoretical and experimental studies have indicated that coaxial nanowire structures could potentially improve the carrier collection and overall efficiency relative to bulk semiconductors of the same materials. Takaguchi and coworkers have reported efficient photoinduced electron transfer processes of single-walled carbon nanotube (SWCNT)/anthryl dendron^{20,40} and SWCNT/fullerodendron^{20,41} supramolecular nanocomposites, of which coaxial nanowire structures provide a photofunctional interface between the SWCNT core and the dendron shell. Interestingly, the charge-separated state of SWCNT/fullerodendron is capable of migrating electron to methyl viologen (MV²⁺) yielding MV^{•+}. Subsequently, the electron pool of MV^{•+} provides electrons to Pt nanoparticles (PVP-Pt) to generate H₂ (Figure 1-19).⁴⁰

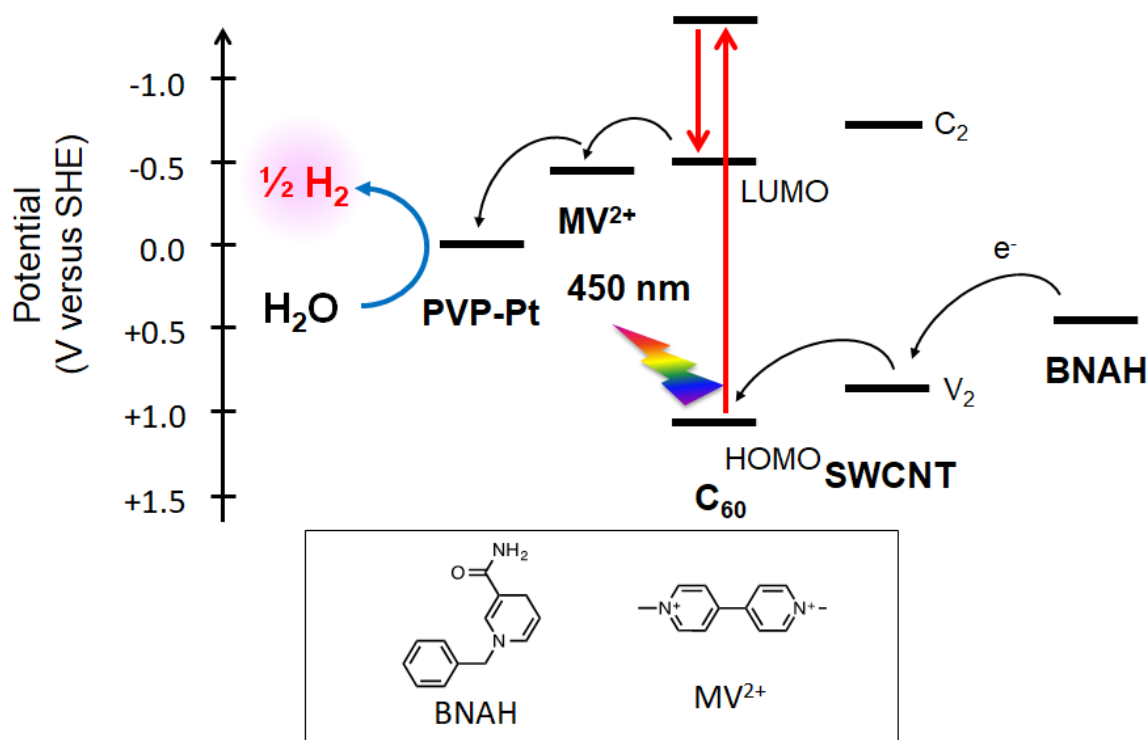


Figure 1-19. Energy-level diagram of photocatalytic H₂ evolution system using SWCNT/fullerodendron as a photosensitizer.

Takaguchi et. al. reported the introduction of Pt(II) complexes into the shell moieties of the coaxial photosensitizer, SWCNT/fullerodendron, since efficient charge migration and inhibition of the charge recombination might be expected.³⁸ Moreover, direct incorporation of Pt(II) co-catalyst into the shell of 6,5-enriched SWCNT/fullerodendron supramolecular composites.³⁹ Upon chirality-selective photo-excitation using monochromatic light ($\lambda = 680$ nm), which is the E₂₂ absorption of (8,3) SWCNTs, we observed the first example for the evolution of H₂ ($\Phi = 0.015$) triggered by the photoexcitation of s-SWCNTs. Then we understand that the fullerodendron plays the important role of a n-type semiconducting material of p/n heterojunction, SWCNT/C₆₀ coaxial heterojunction, showing photocatalytic

activity to produce H_2 from water (Figure 1-20). In order to develop SWCNT/fullerodendron to a practical photocatalyst, the improvement of the efficiency of the SWCNT-photocatalyst is required.

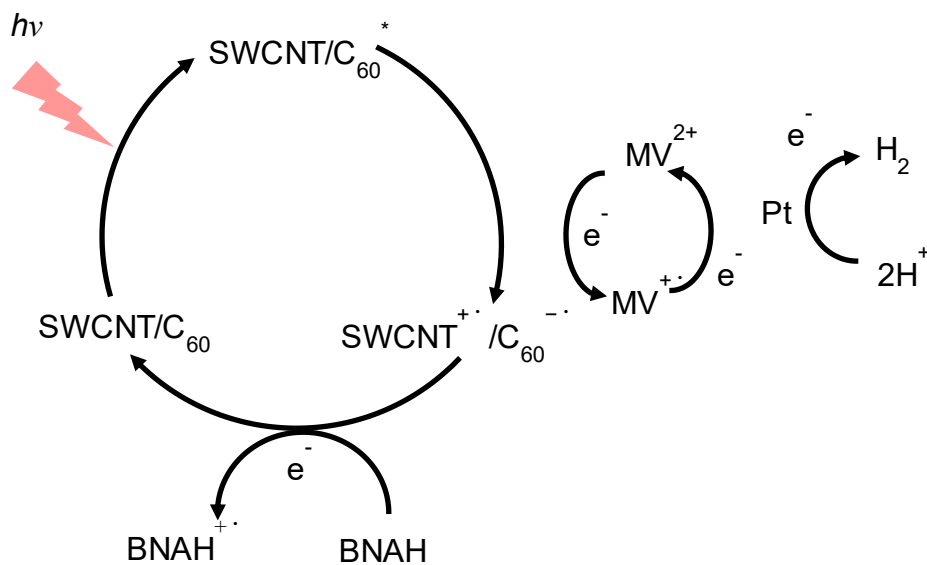


Figure 1-20. Mechanism of hydrogen evolution using the SWCNT-photocatalyst.

4. Why We Introduce TiO_x Layer into the Shell of the SWCNT-photocatalyst

4.1 Transition Metal Oxide (TMO)

As examples of dye-sensitized solar cells or perovskite solar cells, electron extraction layer made of transition metal oxides (TMOs) plays a crucial role for achieving high solar energy conversion efficiency. Meyer et. al. described that TMOs have been used to realize charge-generation junctions for stacked organic light emitting diodes (OLED), sputtering buffer layers for semi-transparent devices, such as organic photovoltaic (OPV) cells.⁴² Fermi

level and conduction band level depend on metals, so it is possible to use the most appropriate metals according to the electron transporting materials (Figure 1-21).⁴²

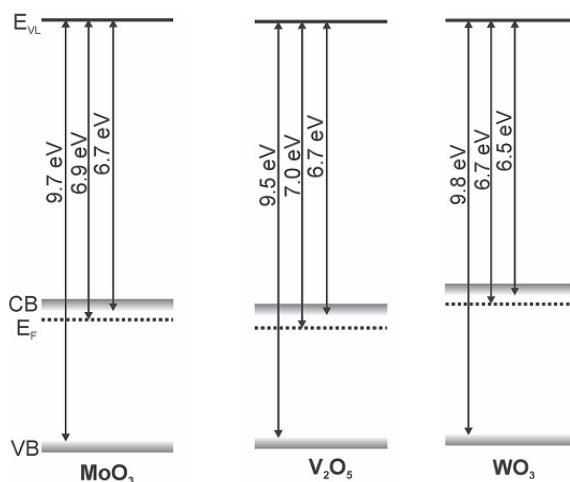


Figure 1-21. CB minimum and VB maximum with respect to the vacuum level (E_{VL}) for MoO₃, V₂O₅ and WO₃.

Titanium oxide (TiO_x), which is produced by the sol-gel condensation of Ti(OPr)₄, is semiconductor materials having a unique set of features which include chemical stability, non-toxicity, low cost, and transparency to visible light. Since TiO_x exhibit conduction band levels that match the LUMOs of the C₆₀-derivatives used in OPVs, TiO_x is used as a promising prospect for electron-transport material.^{43,44} There are two important roles of amorphous titanium oxide (TiO_x).

4.2 Electron-extraction Layer Attained with a Combination of C₆₀ Layer

Waldau et. al. demonstrated OPVs containing interfacial TiO_x layer between active layer of P3HT:PCBM and ITO exhibit improved fill factors(FF) (Figure 1-22).⁴³

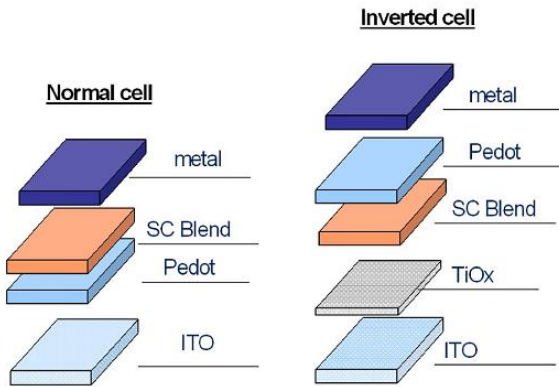


Figure 1-22. The normal OPV is based on ITO/PEDOT:PSS/P3HT:PCBM/LiF/Al (left part of figure) and the inverted OPV is based on ITO/TiO_x/P3HT:PCBM/PEDOT:PSS/Au (right part of figure).

Kubawara et. al. reported very convenient and useful TiO_x thin film, which was fabricated by chemical bath deposition (CBD) method, as the electron extraction-layer of the inverted-type organic solar cell. The ITO/CBD-TiO_x/bis-PCBM:P3HT/PEDOT:PSS/Au device shows an improved short-circuit photocurrent (J_{sc}), open-circuit voltage (V_{oc}), FF, and power-conversion efficiency (η) (Figure 1-23).⁴⁴

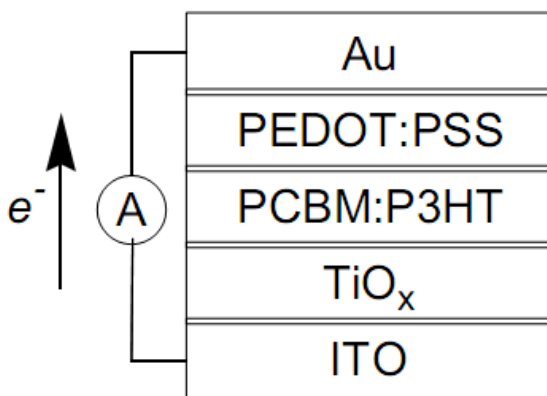


Figure 1-23. Schematic structures of solar cells having CBD-TiO_x layer.

4.3 Hole Blocking Layer for Organic Solar Cells

Hayakawa et. al. reported the TiO_x layer works as an effective barrier to physical damage and chemical degradation, resulting in high durability under aerobic conditions, and also serves as a hole blocking layer, resulting in improved parallel resistance and rectification (Figure 1-24).⁴⁵

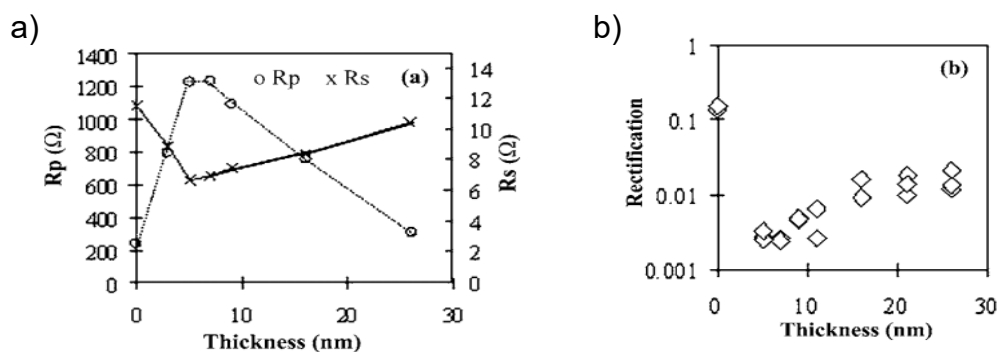


Figure 1-24. a) Series resistance (R_s) and parallel resistance (R_p) of the photovoltaic device with varying thickness of the TiO_x layer b) and their rectification ratio.

In summary, titanium oxide (TiO_x) can enhance solar cells efficiency because of its unique structure and characteristics. This is mainly related to its high chemical stability, intrinsic transparency to visible light (band gap $E_g = 3.2\text{--}3.4\text{ eV}$)⁴⁶ and to the favorable energy level alignment at the solar cell interfaces, which enables an efficient and selective charge carrier uptake and transport (n-type charge transport as a photoanode and/or as a hole-blocking, electron-extraction layer) from the photoactive material to the front transparent electrode of the solar cell.

5. Purpose of This Work

As described above, the recent successful realization of SWCNTs-based solar cells and positive effect of TiO_x on OPVs containing C_{60} as a n-type semiconducting material prompt the author to explore the enhancement the photocatalytic activity of SWCNT/fullerodendron photocatalytic system. A new coaxial photosensitizer with a TiO_x shell as an electron-extraction layer covering a SWCNTs/ C_{60} interface was fabricated to investigate the photocatalytic hydrogen evolution from water. Utilization an electron-extracting TiO_x shell for photocatalytic hydrogen evolution is of an interest because of its capability of acceleration of the electron transfer under concomitant deceleration of the undesirable back electron-transfer (Figure 1-25).

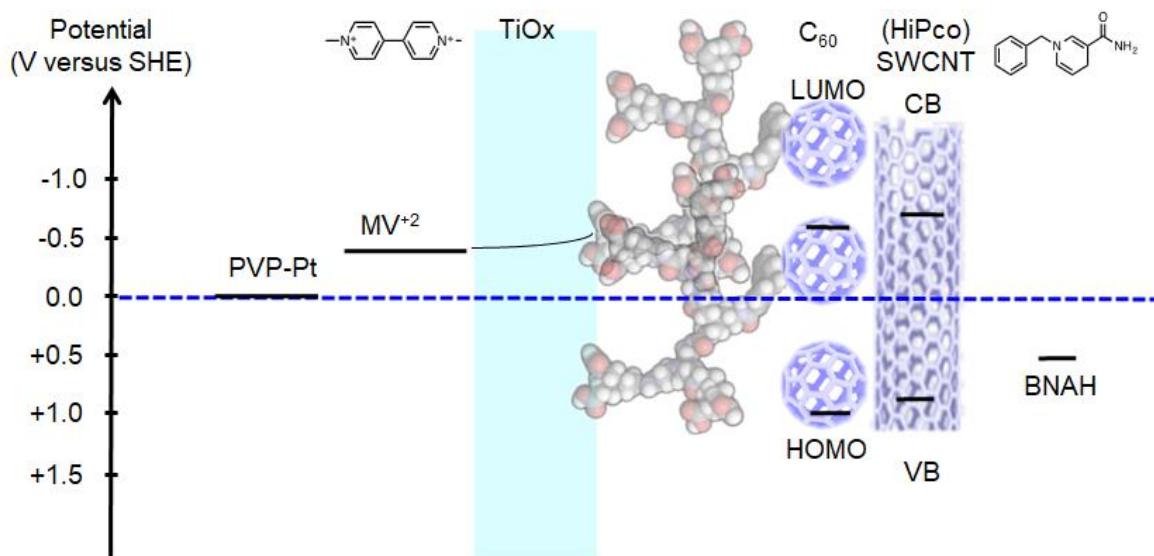


Figure 1-25. An energy-level diagram of the SWCNT/fullerodendron/ TiO_x .

Here we describe the fabrication of SWCNT/fullerodendron/ TiO_x coaxial nano-hybrids that can be used for the effective photocatalytic evolution of hydrogen (Figure 1-26).

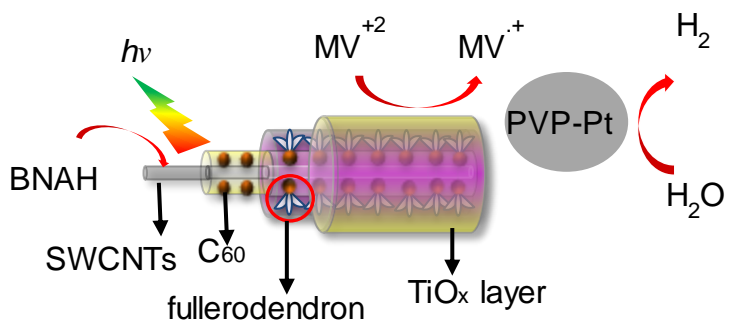


Figure 1-26. Hydrogen generation by SWCNT/fullerodendron/TiO_x and co-catalyst system using xenon lamp ($\lambda = 450$ nm).

References

1. Ravelli, D.; Dondi, D.; Fagnoni, M.; Albini, A. *Chem. Soc. Rev.* **2009**, *38*, 1999.
2. Mao, S. S.; Chen, X. *Int. J. Energy Res.* **2007**, *31*, 619.
3. Kisch, H. *Adv. Photochem.* **2001**, *62*, 93.
4. Chen, X. B.; Shen, S. H.; Guo, L. J.; Mao, S. S. *Chem. Rev.* **2010**, *110*, 6503.
5. (a) Herrmann, J. M. *Catalysis Today* **1999**, *53*, 115; (b) Kisch, H. *Angew. Chem. Int. Ed.* **2013**, *52*, 812.
6. Takanahe, K.; Kamata, K.; Wang, X.; Antonietti, M.; Kubota, J.; Domen, K. *Phys. Chem. Chem. Phys.* **2010**, *12*, 13020.
7. Teri, W. O.; Jin, L. H.; Charles, M. L. *Ann. N.Y. Acad. Sci.* **2002**, *960*, 203.
8. Arnold, M. S.; Green, A. A.; Hulvat, J. F.; Stupp, S. I.; Hersam, M. C. *Nat. Nanotechnol.* **2006**, *1*, 60.
9. Charlier, J. C.; Blase, X.; Roche, S. *Rev. Mod. Phys.* **2007**, *79*, 677.
10. Hong, S.; Myung, S. *Nat. Nanotechnol.* **2007**, *2*, 207.
11. Blackburn, J. *ACS Energy Lett.* **2017**, *2*, 1598.
12. Liu, H.; Nishide, D.; Tanaka, T.; Kataura, H. *Nature Commun.* **2011**, *2*, 309.
13. Charlier, J. C.; Blase, X.; Roche, S. *Rev. Mod. Phys.* **2007**, *79*, 677.
14. Umeyama, T.; Tezuka, N.; Fujita, M.; Hayashi, S.; Kadota, N.; Matano, Y.; Imahori, H. *Chem. Eur. J.* **2008**, *14*, 4875.
15. (a) Ago, H.; Petritsch, K.; Shaffer, M. S. P.; Windle, A. H.; Friend, R. H. *Adv. Mater.* **1999**, *11*, 1281; (b) Star, A.; Stoddart, J. F.; Steuerman, D.; Diehl, M.; Boukai, A.; Wong, E. W.; Yang, X.; Chung, S. -W.; Choi, H.; Heath, J. R. *Angew. Chem.* **2001**, *113*, 1771.

16. Ma, Y.-Z.; Valkunas, L.; Bachilo, S. M.; Fleming, G. R. *J. Phys. Chem. B* **2005**, *109*, 15671.
17. Dukovic, G.; Wang, F.; Song, D.; Sfeir, Y. M.; Heinz, F. T.; Brus, L. E. *Nano Lett.* **2005**, *5*, 2314.
18. Wang, F.; Dukovic, G.; Brus, L. E.; Heinz, T. F. *Science* **2005**, *308*, 838.
19. Maultzsch, J.; Pomraenke, R. S.; Reich, E. C.; Prezzi, D.; Ruini, A.; Molinari, E.; Strano, M. S.; Thomsen, C.; Lienau, C. *Phys. Rev. B* **2005**, *72*, 241402.
20. Takaguchi, Y.; Tamura, M.; Sako, Y.; Yanagimoto, Y.; Tsuboi, S.; Uchida, T.; Shimamura, K.; Kimura, S.; Wakahara, T.; Maeda, Y.; Akasaka, T. *Chem. Lett.* **2005**, *34*, 1608.
21. Umeyama, T.; Tezuka, N.; Seki, S.; Imahori, H. *Adv. Mater.* **2010**, *22*, 1767.
22. Wang, J.; Shea, M. J.; Flach, J. T.; McDonough, T. J.; Way, A. J.; Zanni, M. T.; Arnold, M. S. *J. Phys. Chem. C* **2017**, (DOI:10.1021/acs.jpcc.7b01005).
23. J. F. Nierengarten, *Chem. Eur J.* **2000**, *6*, 3667.
24. Armaroli, N.; Gross, M.; J. F. Nierengarten. *Angew. Chem. Int. Ed.* **1999**, *38*, 3730.
25. Thilgen, C.; Diederich, F. *Science* **1996**, *271*, 317.
26. Tajima, T.; Ohta, K.; Motoyoshiya, J.; Aoyama, H.; Wakahara, T.; Fujitsuka, M.; Asakasa, T.; Ito, O.; Takaguchi, Y. *Angew. Chem. Int. Ed.* **2002**, *41*, 817.
27. Takaguchi, Y.; Sako, Y.; Yanagimoto, Y.; Tsuboi, S.; Motoyoshiya, J.; Aoyama, H.; Wakahara, T.; Akasaka, T. *Tetrahedron Lett.* **2003**, *44*, 5777.
28. Takaguchi, Y.; Yanagimoto, Y.; Tajima, T.; Ohta, K.; Motoyoshiya, J.; Aoyama, H. *Chem. Lett.* **2002**, 1102.
29. Naka, K.; Tanaka, Y.; Chujo, Y. *Chem. Commun.* **1999**, 1931.

30. Naka, K.; Tanaka, Y.; Chujo, Y. *Langmuir* **2002**, *18*, 3655.
31. Naka, K.; Tanaka, Y.; Chujo, Y. *Bull. Chem. Soc. Jpn.* **2002**, *75*, 2541.
32. Naka, K. *Top. Curr. Chem.* **2003**, *228*, 141.
33. Talukdar, B.; Yanagimoto, Y.; Tsuboi, S.; Ichihara, M.; Ohta, K.; Takaguchi, Y. *Bull. Chem. Soc. Jpn.* **2006**, *79*, 1983.
34. Tajima, T.; Tsusi, A.; Fujii, T.; Takada, J.; Takaguchi, Y. *Polymer J.* **2012**, *44*, 620.
35. Nishimura, S.; Tajima, T.; Hasegawa, T.; Tanaka, T.; Takaguchi, Y.; Oaki, Y.; Imai, H.; *Can. J. Chem.* **2017**. Inpress (doi.org/10.1139/cjc-2017-0022).
36. Crooks, R. M.; Zhao, M.; Sun, L.; Chechik, V.; Yeung, L. K. *Acc. Chem. Res.* **2001**, *34*, 3.
37. Sasada, Y.; Tajima, T.; Wada, T.; Uchida, T.; Nishi, M.; Ohkubo, T.; Takaguchi, Y. *New J. Chem.* **2013**, *37*, 4214.
38. Murakami, N.; Tango, Y.; Miyake, H.; Tajima, T.; Nishina, Y.; Kurashige, W.; Neghisi, Y.; Takaguchi, Y. *Sci. Rep.* **2017**, *7*, 43445.
39. Tajima, T.; Sakata, W.; Wada, T.; Tsusui, A.; Nishimoto, S.; Miyake, M.; Takaguchi, Y. *Adv. Mater.* **2011**, *23*, 5750.
40. Sandanayaka, A. S. D.; Takaguchi, Y.; Uchida, T.; Sako, Y.; Morimoto, Y.; Araki, Y.; Ito, O. *Chem. Lett.* **2006**, 1188.
41. Sandanayaka, A. S. D.; Takaguchi, Y.; Sako, Y.; Tamura, M.; Ito, O. *Adv. Sci. Lett.* **2010**, *3*, 353.
42. Meyer, J.; Hamwi, S.; Kröger, M.; Owalsky, W.; Riedl, T.; Kahn, A. *Adv. Mater.* **2012**, *24*, 5408.

43. Waldauf, C. M.; Morana, P.; Denk, P.; Schilinsky, K. C.; Choulis, S. A.; Brabec, C. J. *Appl. Phys. Lett.* **2006**, *89*, 233517.
44. Kuwabara, T.; Nakayama, T.; Uozumi, K.; Yamaguchi, T.; Takahashi, K. *Sol. Energy Mater. Sol. Cells.* **2008**, *92*, 1476.
45. Hayakawa, A.; Yoshikawa, O.; Fujieda, T.; Uehara, K.; Yoshikawa, S. *App. Phys. Lett.* **2007**, *90*, 163517.
46. (a) Partridge, K. S.; Smith, D. K.; Dykes, G. M.; McGrail, P. T. *Chem. Commun.* **2001**, 27, 319; (b) Hirst, A. R.; Smith, D. K. *Org. Biomol. Chem.* **2004**, *2*, 2965.

Chapter 2

Effect of TiO_x Shell on Photocatalytic Activity of the SWCNT- Photocatalyst

2.1 Introduction

The interfaces between metal oxides and organic compounds play an important role in the field of organic electronics, which include organic light-emitting devices (OLEDs),^{1,2} organic photovoltaic cells (OPVs),^{1,3} dye-sensitized solar cells (DSSCs),^{1c} and transistors.⁴ To improve the device performance, these interfaces can often be modified by insertion of a functional interfacial layer. For example, transparent titanium oxide (TiO_x) exhibit electronic levels that match the LUMOs of the C_{60} -derivatives used in OPVs well, which renders TiO_x a promising prospect for electron-transport materials.^{5,6} Waldauf and co-workers have prepared OPVs with an ITO/ TiO_x /RR-P₃HT:PCBM/PEDOT:PSS/Au structure using coating techniques, and demonstrated that these OPVs exhibit improved fill factors (FF).⁵ Kuwabata et al. have reported efficient inverted BHJ solar cells that contain TiO_x as the electron-extraction layer,⁶ which resulted in an improved short-circuit photocurrent (J_{sc}), open-circuit voltage (V_{oc}), FF, and power-conversion efficiency (η).

Meanwhile, coaxial nanowires with a donor-acceptor heterojunction have shown great potential for applications in innovative photofunctional materials. A SWCNTs heterojunction can be constructed from two segments of SWCNTs through topological defects,⁷ such as a pentagon-heptagon (5–7) pair defect,⁸ which could influence the optical, electronic, and mechanical properties of the constituent SWCNTs. Such a heterojunction provides not only an efficient way to design circuits with different electrical properties but also the potential to serve as a functional component in nanodevices,⁹ rectifying diodes,¹⁰ and switches.

SWCNTs are considered ideal supports for photocatalysts because SWCNTs have a large electron storage capability of one electron per 32 carbon atoms that reduces electron-hole recombination have a high specific surface area (SSA) of $1315 \text{ m}^2 \text{ g}^{-1}$ for photocatalyst loading can act as a photosensitizer that enlarges titanium oxide (TiO_x) absorption bandwidth and are transparent layer and highly electrically conducting for efficient electron transport.¹¹⁻¹⁴ From this viewpoint the author exploring a new coaxial photosensitizer with a TiO_x shell as an electron-extraction layer that covers a photo-functional SWCNTs/ C_{60} interface. Here the author describe the fabrication of SWCNT/fullerodendron/ TiO_x coaxial nano-hybrids that can be used for the effective photocatalytical evolution of hydrogen (Figure 2-1).

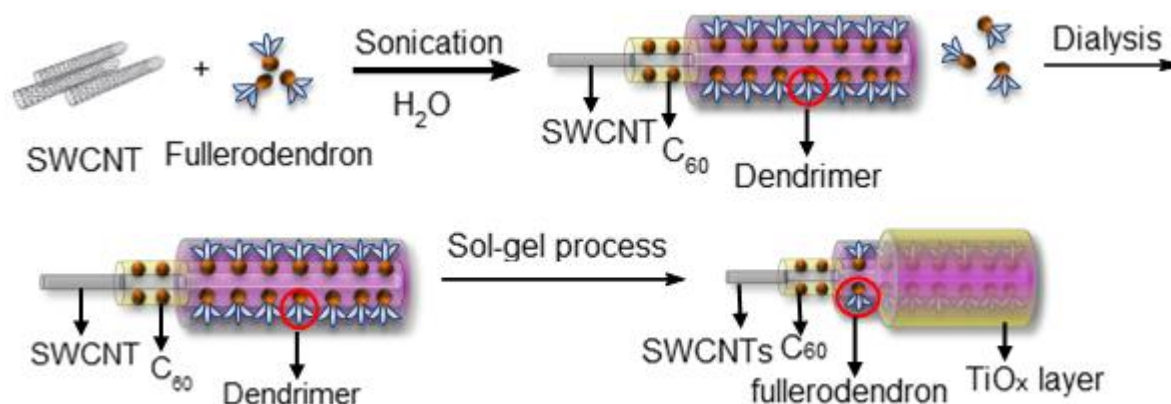


Figure 2-1. Fabrication of SWCNT/fullerodendron/ TiO_x .

2.2 Experimental Section

2.2.1 General

TEM measurements for the composites were conducted using a Hitachi S-5200. The specimens for the measurements were prepared by applying a few drops of the sample solution onto a holey carbon-coated copper grid (Ouken-Shoji 200-Abmesh), and then evaporating the solvent. The absorption data were recorded on a Shimadzu UV-3150 spectrophotometer using a standard cell with a path length of 10 mm. Atomic force microscopy (AFM) observation was carried out using a Seiko SPA 400-DFM and the samples for the observations were prepared by placing a drop of SWCNT/fullerodendron/TiO_x coaxial nanohybrids aqueous solution on freshly cleaved mica, then allowing them to dry with a dryer FT-IR spectra were recorded using Shimadzu IR Affinity-1. Three-dimensional fluorescence spectra data were obtained using a spectrofluorometer (Shimadzu, NIR-PL system). SWCNTs (HiPco) were purchased from Unidym Co. Fullerodendron and SWCNT/fullerodendron supramolecular nanocomposites were prepared according to the reported procedure.¹⁵ All other reagents were purchased from Kanto Kagaku Co., Ltd, Aldrich Chemical Co., and Tokyo Kasei Co., Ltd., and were used as received.

2.2.2 Preparation of SWCNT/fullerodendron supramolecular nanocomposites

SWCNTs (HiPco: 1.0 mg) were placed in a water solution (10 mL) of the fullerodendron (25.5 mg, 0.01 mmol) and then sonicated with a bath type ultrasonifier (ULTRASONIC CLEANER vs-D100, 110 W, 24 kHz) at 17–25 °C for 4 h. After the suspension was centrifuged at 3000 g for 30 min, a black-colored supernatant dispersion, which included SWCNT/fullerodendron supramolecular nanocomposites and superfluous fullerodendron, was collected. The SWCNT/fullerodendron nanocomposites were purified by dialysis for 3 days using dialysis tubing (SPECTRUM RC MEMBRANES Pro 4) to remove superfluous fullerodendron. The dialysis process was continued until the dialysate showed no absorption change at 258 nm in UV-vis spectra. This dialysate solution was used for further experiment as a stock solution of SWCNT/fullerodendron supramolecular nanocomposites.¹⁵

2.2.3 Fabrication of SWCNT/fullerodendron/TiO_x coaxial nanohybrids

An aqueous solution of SWCNT/fullerodendron nanocomposites (1 mL, 0.1 mg SWCNTs) was added by HCl (1.0 N, 2.8 μL) adjust pH ~ 3 then string for 15 min to homogeneous solution. Titanium tetra isopropoxide (TTIP) (5 mg, 1.8×10^{-2} mmol) was dissolved with ethanol (4 mL) then, centrifugation at 4000 rpm for 10 minutes. The supernatant was added to the SWCNT/fullerodendron composite at 0 °C and gently stirred for 24, 48 and 72 h.

2.2.4 Synthesis of Colloidal PVP-Pt

An aqueous solution (10 mL) of $\text{H}_2\text{PtCl}_6 \cdot 6\text{H}_2\text{O}$ (0.034 g, 66 μmol) was dropped into poly(vinylpyrrolidone) (PVP, 0.320 g, $M_w = 40.000 \text{ g/mol}$) in H_2O (20 mL) at room temperature. After diluting with H_2O (20 mL) and ethanol (50 mL), the solution was stirred under reflux conditions for 2 h. After the removal of solvents, the resulting precipitate was dissolved in H_2O (15 mL). After centrifugation at 15000 rpm for 13 h, a clear phase was collected to obtain a colloidal PVP-Pt.

2.2.5 Hydrogen evolution

Typically, 150 mL of an aqueous solution consisting of SWCNT/fullerodendron/ TiO_x (1 mL), Tris-HCl buffer (3.5 mL in H_2O , pH 7.5, 5 mM), methyl viologen dichloride (92.4 mg, 359 μmol), 1-benzyl-1,4-dihydronicotinamide (BNAH) (38.6 mg, 180 μmol), and a colloidal PVP-Pt (15 mL in H_2O , of which Pt atom content was 512 μmol) in a Pyrex reactor was degassed for five cycles and purged with Ar. Upon vigorous stirring at 25 $^\circ\text{C}$, that solution was irradiated with a 300 W Xenon arc light (Ushio model UXL 500 W) through the band-pass filter ($450 \pm 5 \text{ nm}$: ASAHI SPECTRACO, M. C. 450/10 nm 50×50). After a designated period of time, the cell containing the reaction mixture was connected to a gas chromatograph (Shimadzu, TCD, molecular sieve 5A: 2.0 m \times 3.0 mm, Argon carrier gas) to measure the amount of H_2 above the solution. The apparent quantum yield (AQY) is defined as follows. $\text{AQY} = (\text{number of } \text{H}_2 \text{ generated} \times 2)/(\text{number of photons absorbed})$, which was evaluated

from a change in power of the transmitted light, measured using a power meter (Photo-Radio meter Model HD 2302.0 coupled with the irradiance measurement probe LP 471 RAD having an exposure window diameter of 1.6 cm) placed behind the cell parallel to the irradiation cell face.¹⁶

2.3 Preparation SWCNTs Solution for Spray Coating

SWCNTs (1.0 mg) were mixed 1 wt% sodium dodecyl sulfate (SDS) to make SDS dispersion with a concentration of 1 mg/mL. Such suspension was ultrasonically agitated using a probe sonicator with an output sonication power of < 2 W for 4 h followed by centrifugation at 3000 G for 30 min in order to separate out the undissolved SWCNTs bundles and catalyst impurities.

2.3.1 Preparation Thin Film SWCNTs

FTO substrates were cleaned with ethanol:acetone (90 : 10) by sonication process for 30 min, then immersed in the hot ethanol for 10 min, drying FTO substrate with Nitrogen gasses. The FTO substrate was heated in air at 110 °C for 1 h to promote SWCNT/SDS solution were directly spray-coated onto the FTO substrates by using an airbrush pistol. During the spraying process, the FTO substrates were maintained at 110 °C in order to prevent the formation of fine droplets on the surface of the FTO substrates. When the spray process terminated, the films was immersed into deionized water for 24 h to remove the superfluous

SDS surfactant and then dried at 90 °C for 1-2 h. Special care for the choice of the (6,5)-enriched SWCNTs concentration, the nozzle size of the pistol, and the distance from the pistol nozzle to the FTO substrates should be simultaneously done in order to obtain uniform ultrathin SWCNTs films with a high quality.¹⁷

2.3.2 Decoration Thin Film SWCNT with Fullrodendron

An aqueous solution of the fullerodendron (10 mL, 40 μM) was added by 3 μL HCl (1N) to adjust pH ~ 3 then thin film FTO/SWCNT was immersed for 24 h in the fullerodendron acidic solution for decorated surface of thin film FTO/SWCNTs. Therefore rinsed thin film FTO/SWCNT/fullerodendron in the water surface for 3 time to removal from superfluous of fullerodendron on the surface.

2.3.3 Decoration TiO_x on the Surface of Thin Film SWCNT/fullerodendron

Titanium tetra isopropoxide (TTIP) (5 mg, 1.8×10^{-2} mmol) was dissolved with ethanol (4 mL) then, centrifugation at 4000 rpm for 10 minutes. Then pipette supernatant 20 μL and was dropped into spin-coated on the substrate in air at 1000 rpm for 60 s and kept in the ambient at room temperature for 1 h. A thermal treatment at 85 °C for 10 min was observed to be beneficial for the device performance.

2.4 Results and discussion

2.4.1 Fabrication of SWCNT/fullerodendron/TiO_x

SWCNT/fullerodendron/TiO_x nano-hybrids were fabricated by polycondensation reaction of titanium tetra isopropoxide (TTIP)¹⁸ using SWCNT/fullerodendron supramolecular nano-composites as catalytic scaffolds according to previous reports on SWCNT/fullerodendron/SiO₂ nano-hybrids.¹⁹ In a typical run, HCl (1.0 N, 2.8 μL) was added to an aqueous solution of SWCNT/fullerodendron nano-composites (1 mL). Subsequently, TTIP (20 μL, 0.17 mM) in ethanol was added to the solution at 0 °C. After gentle stirring for 24, 48, and 72 h, a dispersion of SWCNT/fullerodendron/TiO_x was obtained.

2.4.2 Characterization of SWCNT/fullerodendron/TiO_x

a) Scanning Electron Microscopy (SEM)

The morphology of the SWCNT/fullerodendron/TiO_x nano hybrids was examined by scanning electron microscopy (SEM). Here we shown SEM images SWCNT/fullerodendron/TiO_x after sol-gel reaction for 24, 48 and 72 h. The tiny fibers with 1–3 μm length and 60–120 nm diameters were observed after sol-gel reaction for 48 h. Thickness of the very thin nanofiber shown in the white rectangle in Figure 2-2 is ca. 50 nm.

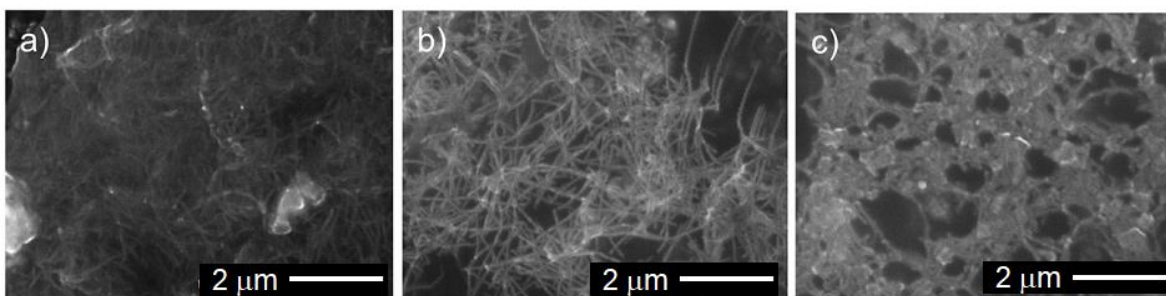


Figure 2-2. The shell thickness affecting the photoactivity.

b) Transmission Electron Microscopy (TEM)

The TEM images prepared in the water solution containing SWCNT/fullerodendron/TiO_x coaxial nano-hybrids. In addition to a clear coaxial nanowires structure of SWCNT/fullerodendron/TiO_x that a uniformly thick shell composed of nano-sized TiO_x covered the SWCNT/fullerodendron nano-wire with 50 nm wide (Figure 2-3).

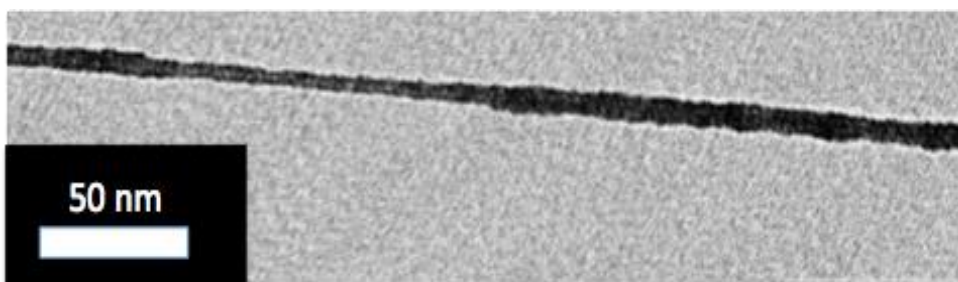


Figure 2-3. TEM image of SWCNT/fullerodendron/TiO_x supramolecular nanohybrids.

c) Atomic Force Microscopy (AFM)

Atomic force microscopy (AFM) is a classic technique for characterising SWCNTs and provides vital information on their diameter, length and degree of individualisation. When studying the dispersion quality using AFM, attention usually focuses only on the linear features associated with the SWCNTs. Other non-SWCNTs species are often simply assigned as impurities, such as amorphous carbon or catalyst particles inherited from SWCNTs synthesis.²⁰

In addition the height profiles in the AFM analysis revealed that the thickness of SWCNT/fullerodendron/TiO_x coaxial nano-hybrids (~15 nm) is higher than that of the SWCNT/fullerodendron supramolecular nano-composite (2-3 nm) (Figure 2-4). Based on these results, the thickness of the TiO_x layer was estimated to be 6-7 nm. These observations are consistent with the SWCNT/fullerodendron/TiO_x coaxial nano-hybrid structure, the SWCNT-core surrounded by the fullerodendrons, coated by the outer TiO_x shell (Figure 2-5).

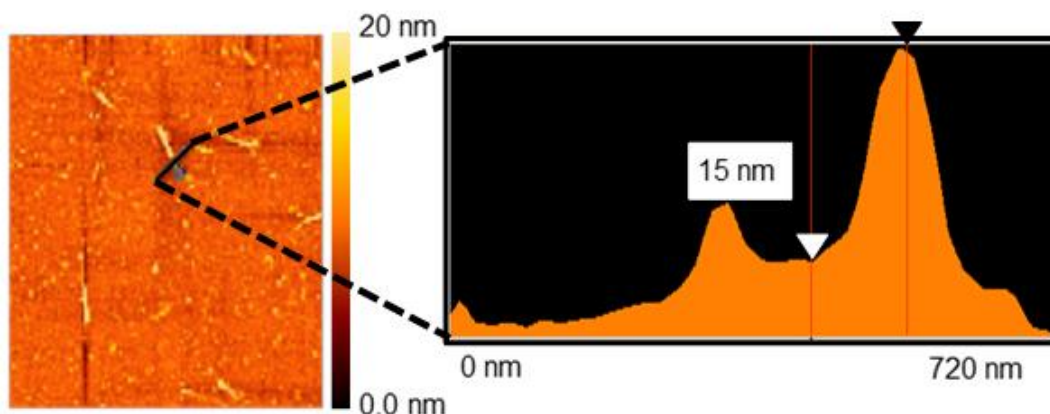


Figure 2-4. AFM image of SWCNT/fullerodendron/TiO_x supramolecular nanohybrids.

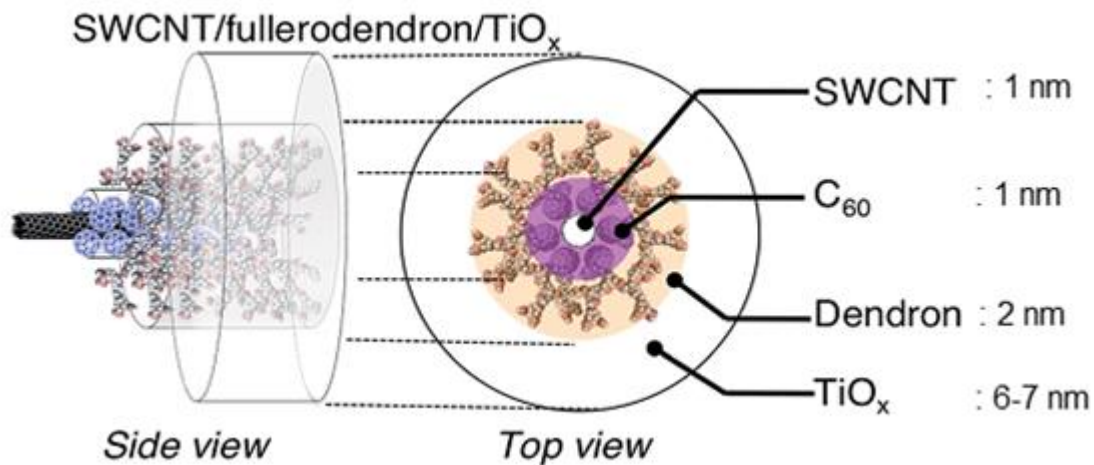


Figure 2-5. Confirmation thickness of each layer in the SWCNT/fullerodendron/TiO_x.

d) Photoluminescence Mapping of SWCNT/Fullerodendron/TiO_x

The photoluminescence of SWCNTs is consistent with isolated SWCNTs and therefore characterization of isolated SWNTs is possible. Individual SWCNTs dissolved in a surfactant solution exhibit photoluminescence in the near-IR region.²¹ The coaxial nanowire structure with isolated SWCNTs was confirmed by three-dimensional photoluminescence (PL) intensity mapping in D₂O, allowed assigning four intense peaks with reasonable certainty to the (9,4), (8,6), (7,6), and (8,4) SWCNTs.²² It should be noted that the coaxial structure is maintained, i.e., the formation of bundles and/or aggregation of the SWCNTs after the formation of the SWCNT/fullerodendron/TiO_x coaxial nano-hybrids was not observed (Figure 2-6).

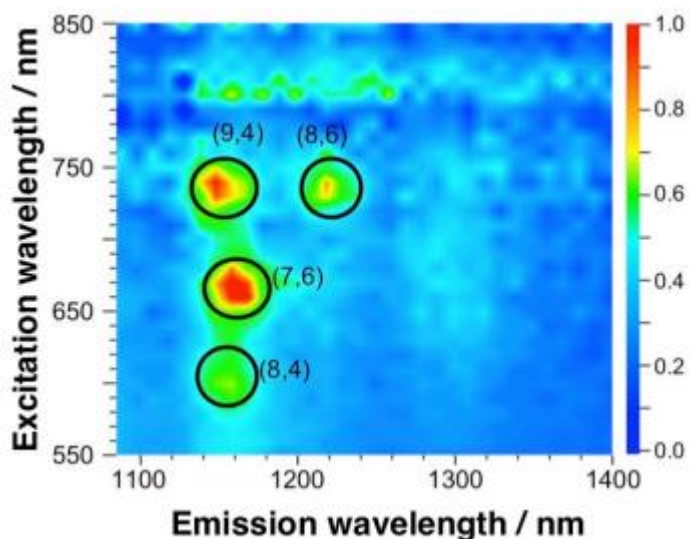


Figure 2-6. Three-dimensional fluorescence spectra of SWCNT/fullerodendron/TiO_x coaxial nano hybrids.

e) Spectroscopy Visible-Near Infrared (NIR)

Confirmation layer the TiO_x layer of the SWCNT/fullerodendron/TiO_x nano hybrid shows high optical transparency in the visible and near infrared (NIR) region. (Figure 2-7) shows the Vis-NIR absorption spectra of the SWCNT/fullerodendron supramolecular nanocomposites and the SWCNT/fullerodendron/TiO_x coaxial nano hybrids. The absorption of the SWCNT/ fullerodendron/TiO_x coaxial nano-hybrids is smaller than that of the SWCNT/fullerodendron composites, as the concentration of the SWCNT/fullerodendron/TiO_x coaxial nano-hybrids was lowered during the sol-gel condensation process. However, the absorption and/or scattering due to the TiO_x layer on the shell should be negligible on account of the nano-sized thickness of the TiO_x layer. From the

comparison of absorption bands (500-1350 nm) before and after the sol-gel condensation, we can be found four kinds of type SWCNTs such as (9,4), (8,6), (7,6), and (8,4) that allowed assigned in the photoluminescence (PL) mapping spectra.²²

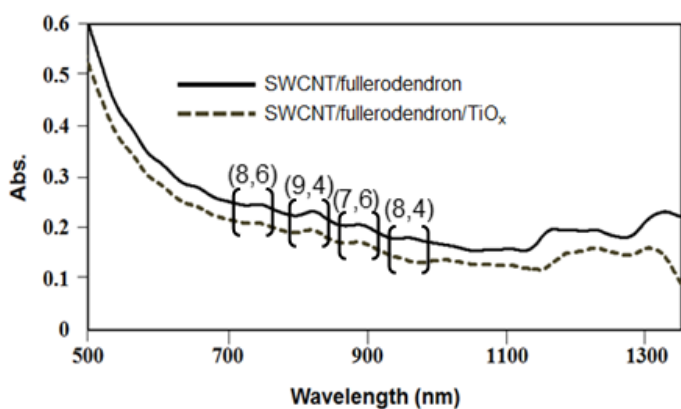


Figure 2-7. Vis-NIR spectra of SWCNT/fullerodendron supramolecular nanocomposites and SWCNT/ fullerodendron/TiO_x coaxial nano hybrids.

f) Infrared Spectra of SWCNT/fullerodendron/TiO_x

To obtain a better understanding of the fullerodendron/TiO_x junction, FTIR spectroscopic measurements of the SWCNT/fullerodendron/TiO_x nano-hybrid were conducted (Figure 2-8). The IR spectra of the SWCNT/fullerodendron/TiO_x nano hybrids exhibit the C=O stretching modes at 1725 cm⁻¹, which is shifted toward higher frequencies than those of the SWCNT/fullerodendron supramolecular nano-composites (1680 cm⁻¹). This result indicates the formation of Ti-OCOR bonds at the termini of the fullerodendrons.²³ The sharp absorption band observed at 635 cm⁻¹ was ascribed to the Ti-O-Ti moieties, while the strong

absorption band at 1055 cm^{-1} was attributed to the Ti-O-C stretching mode. Based on these observations, we concluded that the TiO_x layer is attached onto the surface the SWCNT/fullerodendron supramolecular nano-composites without significant damage to the

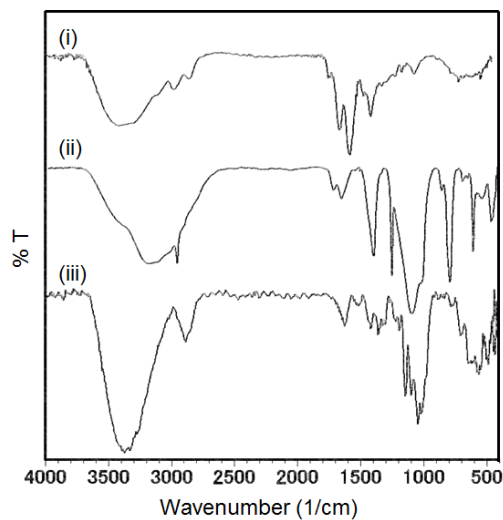


Figure 2-8. IR spectra of (i) SWCNT/fullerodendron, (ii) SWCNT/fullerodendron/ TiO_x and (iii) TiO_x .

g) Raman Spectra of SWCNT/fullerodendron/ TiO_x

Raman scattering is well known as an important technique to characterize the different form of carbon material. Recently, the resonance Raman scattering (RRS) technique has been shown to provide a powerful tool for studying and characterizing single-walled carbon nanotubes (SWCNTs), first for bundles and recently for isolated SWCNTs.²⁴ In addition to clear a Raman spectrum of the SWCNT/fullerodendron/ TiO_x coaxial nano-hybrids showed

typical scattering of the disorder induced mode (D) and the tangential displacement mode (TDM; also called the G band), which were observed at 1339 and 1610 cm^{-1} , respectively (Figure 2-9).^{25,26} The very small intensity of the D-band indicates that the SWCNTs within the composites did not sustain any substantial damage. Broad peaks at 610 and 425 cm^{-1} were ascribed to TiO_x .²⁷

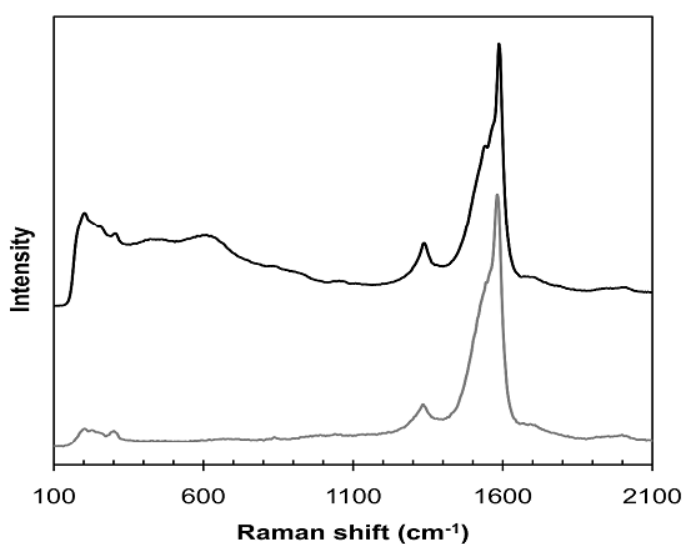


Figure 2-9. Raman spectra for SWCNT/fullerodendron (Gray line) and SWCNT/fullerodendron/ TiO_x (black line).

2.4.3 Application of SWCNT/fullerodendron/ TiO_x Coaxial Nano-hybrids

2.4.3.1 Hydrogen Evolution from SWCNT/fullerodendron/ TiO_x

To probe the beneficial aspects of the incorporation of the transparent electron-extraction layer into an SWCNT/fullerodendron coaxial photosensitizer, we explored the photocatalytic

evolution of hydrogen from water using a system based on the SWCNT/fullerodendron/TiO_x supramolecular nano-composites coupled with colloidal poly(vinylpyrrolidone)-platinum (PVP-Pt). The plots of the total amount (4.0 μmol/h) proceeded steadily and an induction period or decreasing activity was not observed during 6 h of irradiation. Although the SWCNT/fullerodendron supramolecular nanocomposites also worked as a photosensitizer for the evolution of hydrogen, the reaction rate of the hydrogen generation (1.9 μmol/h) is lower than that of SWCNT/fullerodendron/TiO_x nano hybrids (4.0 μmol/h). Given that the absorbance of the SWCNT/fullerodendron/TiO_x nano-hybrids is lower than that of the SWCNT/fullerodendron supramolecular nano-composites, the photocatalytic activity of the SWCNT/fullerodendron/TiO_x nano-hybrids must be higher than that of the SWCNT/fullerodendron supramolecular nano-composites. In order to compare the efficiency of the photocatalytic evolution of hydrogen between the SWCNT/ fullerodendron supramolecular nano composite and the SWCNT/fullerodendron/TiO_x nano-hybrids photocatalysts, we evaluated their quantum yields by using monochromic light ($\lambda = 450 \pm 5$ nm), which revealed apparent quantum yields (AQYs) for the evolution of hydrogen ($2 \times$ number of molecules of hydrogen generated/number of photons absorbed) of 0.47 (SWCNT/fullerodendron/TiO_x) and 0.12 (SWCNT/fullerodendron) (Figure 2-10).

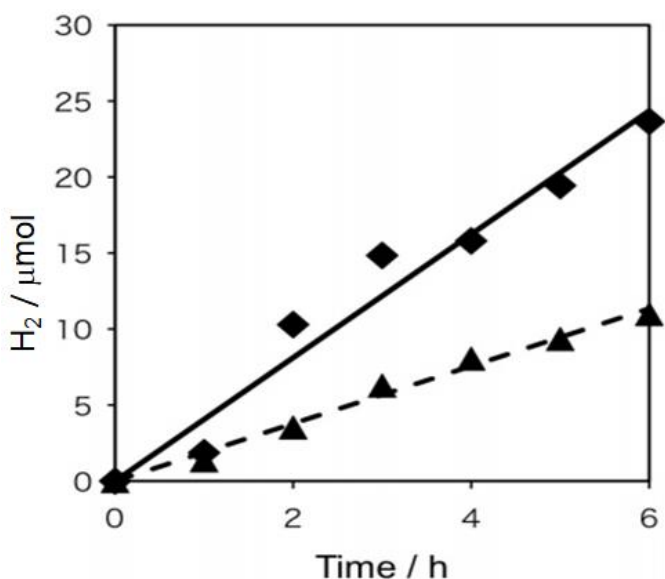


Figure 2-10. Time dependence of the evolution of hydrogen from water using SWCNT/fullerodendron (\blacktriangle) or SWCNT/fullerodendron/TiO_x (\blacklozenge).

2.5 Energy-level diagram of the SWCNT/fullerodendron/TiO_x

An energy-level diagram of the conduction (C_1 and C_2) and valence bands (V_1 and V_2) of (7,6) SWCNT,²⁸ which is one of the most commonly encountered types of CNTs in HiPco, together with the LUMO levels of C₆₀,²⁹ MV²⁺,³⁰ BNAH,³¹ and the energy level of Pt and TiO_x is shown in (Figure 2-11). A distinctive advantage of the coaxial architecture is that the carrier separation occurs in the shorter radial direction as opposed to the longer axial direction. Moreover, the energy-level diagram indicates that the electron-extraction layer of TiO_x not only decelerates the electron back-transfer, but also accelerates the electron forward-transfer from the conduction band of TiO_x to the LUMO of MV²⁺, thus leading to an efficient electron-transfer pathway.

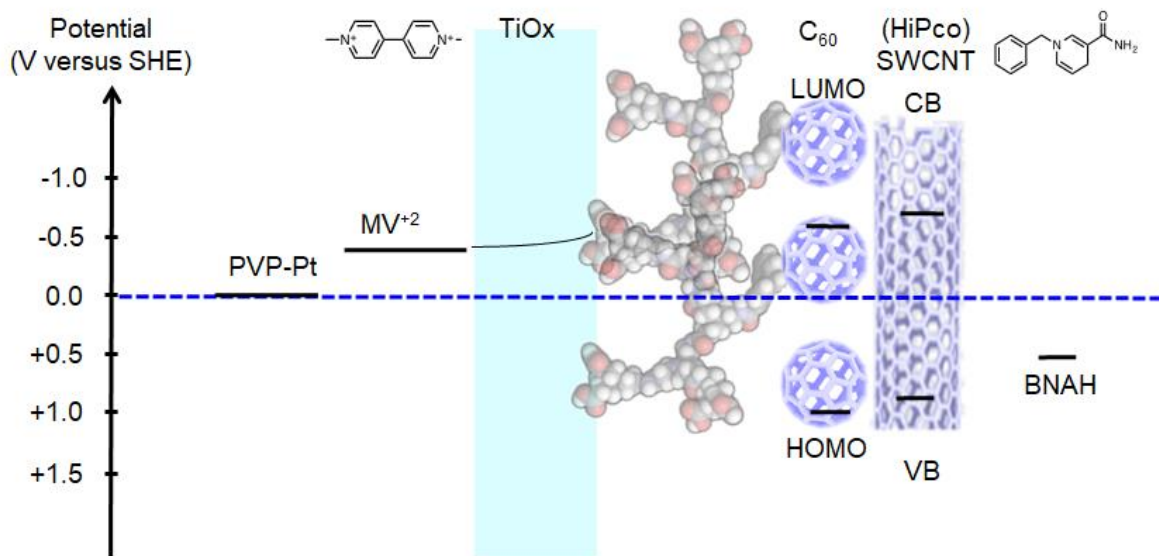


Figure 2-11. Energy-level diagram of the SWCNT/fullerodendron/TiO_x coaxial photocatalyst system.

2.6 Fabrication Thin Film FTO/SWCNT/fullerodendron/TiO_x

Thin film FTO/SWCNT/fullerodendron/TiO_x was fabricated by spray coating dispersion of SWCNT (1.0 mg) in the SDS solution (1 wt%). During the spray coating process, the FTO substrates were maintained at 110 °C in order to prevent the formation of fine droplets on the surface of the FTO substrates. When the spray process terminated, the films were immersed into deionized water for 24 h to remove the superfluous SDS surfactant and then dried at 90 °C for 1-2 h. The obtained films were immersed in an aqueous solution of fullerodendron to decorate the surface of the film photocathode with fullerodendron. The photocathode was decorated with TiO_x by the polycondensation reaction of titanium tetra isopropoxide (TTIP).

2.6.1 Hydrogen Evolution from Thin Film SWCNT/fullerodendron/TiO_x

A steady generation of H₂ generation from recycles used of the thin film FTO/SWCNT/fullerodendron/TiO_x first used (1.82 μmol/h) and second used (1.48 μmol/h) was observed upon exposure to a light of wavelength 422 ± 5 nm with a 300 W Xenon arc lamp (Figure 2-12). It is notable that 81% of H₂-evolving activity was remained for the second use of a spray-coated film of SWCNT/fullerodendron/TiO_x on a FTO plate coupled with colloidal poly(vinylpyrrolidone)platinum (PVP-Pt) after the 6 hour H₂ evolution reaction.

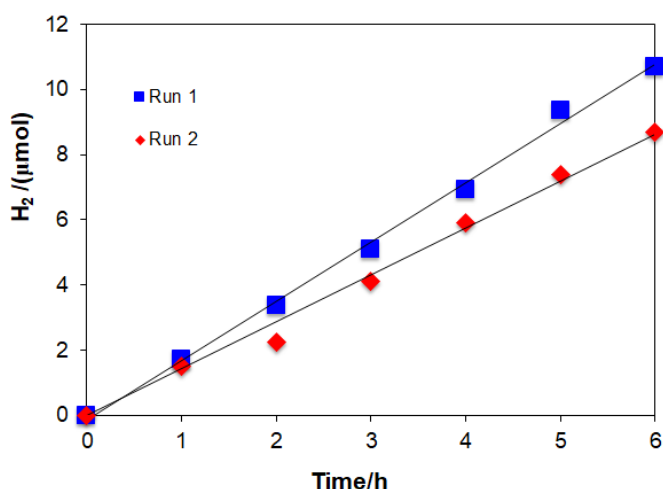


Figure 2-12. Time dependencies of the H₂ production from water in the systems of recycle use of the thin film FTO/SWCNT/fullerodendron/TiO_x catalyzed by a colloidal PVP-Pt. Thin film FTO/SWCNT/fullerodendron/TiO_x first used (■) and second used (◊).

2.6.2 Photoelectrode Hydrogen Evolution

The photoelectrochemical measurements were carried out in a typical three-electrode electrochemical cell under Xenon lamp ($\lambda > 422$ nm). The as-prepared photoelectrode thin film FTO/SWCNT/fullerodendron/TiO_x act as working electrode, Ag/AgCl as reference electrode, and Pt wire were used as the counter electrode, respectively. The photoelectrode measurements were conducted in 0.1 M Na₂SO₄/NaOH solution (pH = 7). The result show that enhancement of the photoelectrode thin film FTO/SWCNT/fullerodendron/TiO_x can be evaluated hydrogen at wavelength 550 nm (green light) and also at 650 nm (red light) using bias potential 0.3 V (Vs Ag/AgCl).

2.7 Summary

A bespoke SWCNTs photocatalyst with an electron-extracting TiO_x shell was fabricated. On account of the presence of the TiO_x shell, the SWCNT/fullerodendron/TiO_x coaxial nanowire exhibits a high activity in the catalytic evolution of H₂ from water under irradiation with visible light, because the electron-extracting TiO_x layer accelerates the electron forward-transfer under concomitant deceleration of the undesirable back electron-transfer (Figure 2-13). Incorporations of the TiO_x electron-extraction layer to the p-n heterojunction consisting of s-SWCNT (p-type) and C₆₀ (n-type) is very useful and efficient to provide anionic lateral surface to improve efficiency photocatalytic H₂ evolution from water, make robustness thin film based on SWCNT/C₆₀, fullerodendron and TiO_x.

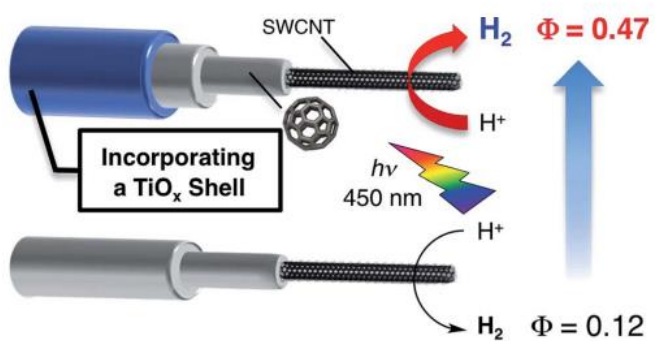


Figure 2-13. Efficiency TiO_x shell to enhance photocatalytic hydrogen evolution from water under visible light.

References

1. For reviews, see: (a) Meyer, J.; Hamwi, S.; Kröger, M.; Kowalsky, W.; Riedl, T.; Kahn, A. *Adv. Mater.* **2012**, *24*, 5408; (b) Zilberberg, K.; Meyer, J.; Riedl, T. *J. Mater. Chem. C.* **2013**, *1*, 4796; (c) Ratcliff, E. L.; Zacher, B.; Armsrong, N. R. *J. Phys, Chem. Lett.* **2011**, *2*, 1337.
2. (a) Tokito, S.; Noda, K.; Taga, Y. *J. Phys. D: Appl. Phys.* **1996**, *29*, 2750; (b) Kanno, H.; Holmes, R. J.; Sun, Y.; Kena-Cohen, S.; Forrest, S. R. *Adv. Mater.* **2006**, *18*, 339; (c) Reynold, K. J.; Barker, J. A.; Greenham, N. C.; Friend, R. H.; Frey, G. L. *J. Appl. Phys.* **2002**, *92*, 7556; (d) Chu, C.-W.; Chen, C.-W.; Li, S.-H.; Wu, E. H. -E.; Yang, Y. *Appl. Phys. Lett.* **2005**, *86*, 253503; (e) You, H.; Dai, Y.; Zhang Z.; Ma, D. *J. Appl. Phys.* **2007**, *101*, 026105; (f) Meyer, J.; Hamwi, S.; Kröger, M.; Kowalsky, W.; Riedl, T.; Kahn, A. *Adv. Mater.* **2012**, *24*, 5408; (g) Bolink, H. J.; Coronado, E.; Repetto, D.; Sessolo, M.; Barea, E. M.; Bisquert, J.; Garcia-Belmonte, G.; Prochazka, J.; Kavan, L. *Adv. Funct. Mater.* **2008**, *18*, 145.
3. For reviews, see: (a) Wang, F.; Tan, Z.; Li, Y. *Energy Environ. Sci.* **2015**, *8*, 1059; (b) Chen, S.; Manders, J. R.; Tsang, S.-W.; So, F. *J. Mater. Chem.* **2012**, *22*, 24202.
4. Cho, S.; Seo, J. H.; Lee, K.; Heeger, A. J. *Adv. Funct. Mater.* **2009**, *19*, 1459.
5. Waldauf, C.; Morana, M.; Denk, P.; Schilinsky, P.; Coakley, K.; Choulis, S. A.; Brabec, C. *J. Appl. Phys. Lett.* **2006**, *89*, 233517.
6. Kuwabara, T.; Nakayama, T.; Uozumi, K.; Yamaguchi, T.; Takahashi, K. *Sol. Energy Mater. Sol. Cells*, **2008**, *92*, 1476.
7. Wu, G.; Li, B. *Phys. Rev. B* **2007**, *76*, 085424.
8. Ebbesen, T. W.; Takaada, T. *Carbon* **1995**, *33*, 973.

9. Bandaru, P. R.; Daraio, C.; Jin, S.; Rao, A. M. *Nature Mater.* **2005**, *4*, 663.
10. Yao, Z.; Postma, H. W. C.; Balents, L.; Dekker, C. *Nature* **1999**, *402*, 273.
11. Kongkanan, A.; Kamat, P. V. *ACS Nano* **2007**, *1*, 13.
12. Martel, R.; Schmidt, T.; Shea, H. R.; Hertel, T.; Avouris, P. *Appl. Phys. Lett.* **1998**, *73*, 2447.
13. Peigney, A.; Laurent, C.; Flahaut, E.; Bacsa, R. R.; Rousset, A. *Carbon* **2001**, *39*, 507.
14. Woan, K.; Pyrgiotakis, G.; Sigmund, W. *Adv. Mater.* **2009**, *21*, 2233.
15. Takaguchi, Y.; Tamura, M.; Sako, Y.; Yanagimoto, Y.; Tsuboi, S.; Uchida, T.; Shimamura, K.; Kimura, S.; Wakahara, T.; Maeda, Y.; Akasaka, T. *Chem. Lett.* **2005**, *34*, 1608.
16. Sasada, Y.; Tajima, T.; Wada, T.; Uchida, T.; Nishi, M.; Ohkubo, T.; Takaguchi, Y. *New J. Chem.* **2013**, *37*, 4214.
17. Liu, Q.; Fujigaya, T.; Cheng, H. M.; Nakashima, N. *J. Am. Chem. Soc.* **2010**, *132*, 16581.
18. Pasquarelli, R. M.; Ginley, D. S.; O'Hayre, R. *Chem. Soc. Rev.* **2011**, *40*, 5406.
19. Tajima, T.; Sakata, W.; Wada, T.; Tsusui, A.; Nishimoto, S.; Miyake, M.; Takaguchi, Y. *Adv. Mater.* **2011**, *23*, 5750.
20. Yau, H. C.; Bayazit, M. K.; Steinke, J. H. G.; Shaffer, M. S. P. *Chem. Commun.* **2015**, *51*, 16621.
21. a) O'Connell, M. J.; Bachilo, S. M.; Huffman, C. B.; Moore, V. C.; Strano, M. S.; Haroz, E. H.; Rialon, K. L.; Boul, P. J.; Noon, W. H.; Kittrell, C.; Ma, J.; Hauge, R. H.; Weisman, R. B.; Smalley, R. E. *Science* **2002**, *297*, 593; b) Bachilo, S. M.; Strano, M. S.; Kittrell, C.; Hauge, R. H.; Smalley, R. E.; Weisman, R. B. *Science* **2002**, *298*, 2361.
22. Liu, H.; Nishide, D.; Tanaka, T.; Kataura, H. *Nature Commun.* **2011**, *2*, 309.

23. Perrin, F. X.; Nguyen, V.; Vernet, J. L. *J. Sol-Gel Sci. Technol.* **2003**, 28, 205.
24. Jario, A.; Filho, A. G. S.; Dresselhaus, M. S.; Dresselhaus, G.; Swan, A. K.; Unlu, M. S.; Goldberg, B. B.; Pimenta, M. A.; Hafner, J. A.; Lieber, J. M.; Sato, R. *Mat. Res. Soc. Symp. Proc.* **2002**, 706.
25. Jeníková, M.; Zakuťanská, K.; Kováča, J.; Girman, V.; Kopčanský, P.; Tomašovičová, N. *Acta Phys. Polonica A.* **2016**, (DOI: 10.12693/APhysPolA.131.952).
26. Dresselhaus, M. S.; Dresselhaus, G.; Saito, R.; Jorio, A. *Phys. Rep.* **2005**, 47, 409.
27. Wen, Z.; Ci, S.; Mao, S.; Cui, S.; Lu, G.; Yu, K.; Luo, S.; He, Z.; Chen, J. *J. Power Sources* **2013**, 234, 100.
28. Tanaka, Y.; Hirano, Y.; Niidome, Y.; Kato, K.; Saito, S.; Nakashima, N. *Angew. Chem. Int. Ed.* **2009**, 48, 7655.
29. Takaguchi, Y.; Sako, Y.; Yanagimoto, Y.; Tsuboi, S.; Motoyoshiya, J.; Aoyama, H.; Wakahara, T.; Akasaka, T. *Tetrahedron Lett.* **2003**, 44, 5777.
30. Ito, M.; Kuwana, T. *Electroanal. Chem.* **1971**, 32, 415.
31. Zhu, X. Q.; Zhang, M. T.; Yu, A.; Wang, C. H.; Cheng, J. P. *J. Am. Chem. Soc.* **2008**, 130, 2501.

Chapter 3

Conclusion

Conclusion

Incorporations of the TiO_x electron-extraction layer to the p-n heterojunction consisting of s-SWCNT (p-type) and C_{60} (n-type) is very useful and efficient to fabricate the SWCNT-photocatalyst and the SWCNT-photoelectrode generating H_2 from water. In this thesis, the author has shown that the dendrimer assisted sol-gel condensation of the titanium tetraisopropoxide (TTIP) is an effective method to incorporate the electron-extraction layer to the SWCNT/ C_{60} heterojunction. In addition, this strategy is quite effective not only to enhance the photocatalytic H_2 evolution activity of SWCNT/fullerodendron nanocomposite but also to stabilize the individual coaxial heterojunction or the SWCNT/ C_{60} film structure (Figure 4-1).

For example, the author described the new coaxial photosensitizer with the electron-extraction TiO_x shell covering a SWCNTs/ C_{60} interface in chapter 2. On account of the presence of the TiO_x shell, the SWCNT/fullerodendron/ TiO_x coaxial nanowire exhibits a high activity ($\Phi = 0.47$), which is 3.9 times higher than that of SWCNT/fullerodendron, in the catalytic evolution of H_2 from water under irradiation with visible light. This result provides the evidence, i.e., the electron-extracting TiO_x layer accelerates the electron forward-transfer under concomitant deceleration of the undesirable back electron-transfer. As shown in Figure 4-1, introducing a TiO_x -layer improves H_2 evolution efficiency.

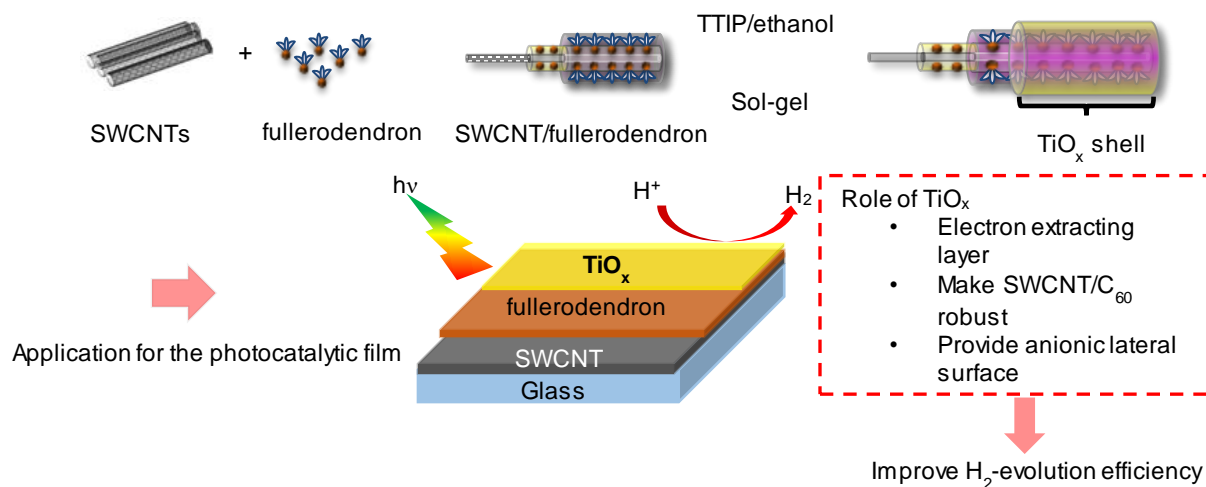


Figure 4-1. Introduction of the TiO_x shell on the coaxial SCWNT/C₆₀ heterojunction.

Furthermore, the author found an alternative and simple method for the fabrication of a robust film possessing the SWCNT/C₆₀ heterojunction decorated with TiO_x-layer. The photoelectrode thin film FTO/SWCNT/fullerodendron/TiO_x displayed photoelectrochemical water splitting in an aqueous electrolyte solution with a negative onset potential of -0.3 V vs. Ag/AgCl, which is 0.1 V more positive in comparison to a SWCNT electrode. Importantly, the film shows higher stability against the bias voltages compared to the FTO/(6,5) enriched SWCNT/fullerodendron. Fabrication of a photoelectrode film based on SCWNT/C₆₀ shown in the Figure 4-2.

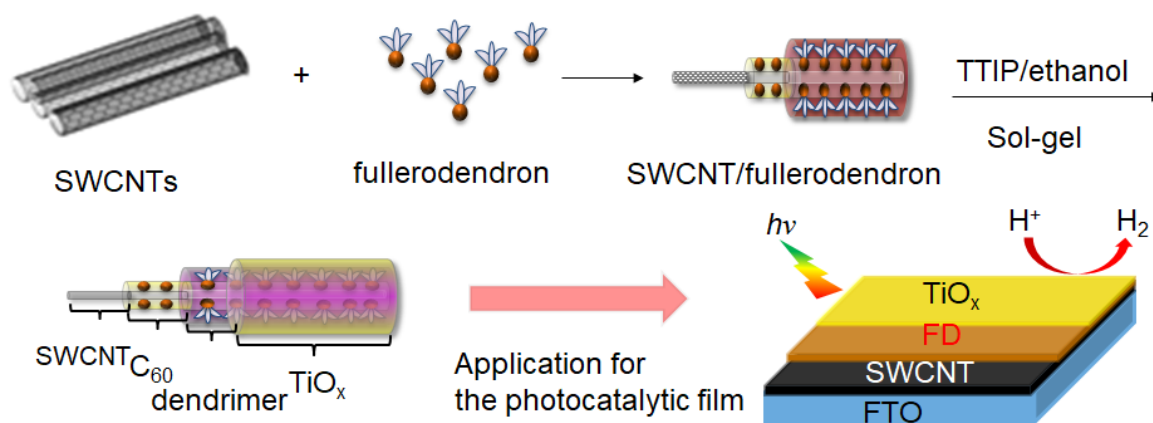


Figure 4-2. Introduction of the TiO_x-layer on the top of SWCNT/C₆₀ heterojunction film.

Enhancement various kinds of organic and inorganic coaxial nanowires have been developed so far, coaxial nanowire photocatalysts consisting of (p-type semiconductor)/(n-type semiconductor)/(electron-extraction layer) are still in the early stages of development, mostly due to their relatively complicated fabrication procedures. Here, the fabrication technique described in this thesis provides a versatile method to produce a wide variety of coaxial heterojunction structures and film devices. The dendron unit functions as effective “glue” between the carbon materials and electron extract layer and enables the facile formation or fabrication of photofunctional materials. Incorporating an electron-extracting layer to nanocarbon materials described in this thesis should be an effective strategy toward further challenging photofunctional materials based on CNTs.

Acknowledgement

This work was performed at Graduate School of Environmental and Life Science of Okayama University under the supervision of Dr. Yutaka Takaguchi during period October 2014 to September 2017.

I would like to thank to Dr. Yutaka Takaguchi for providing me with the opportunity to work on this research project as well as for continuously having a new and exciting ideas and for his inspiring approach for the chemistry.

I wish to express my sincerest gratitude to Dr. Tomoyuki Tajima of Okayama University for his valuable suggestion, numerous discussions and warm encouragement.

I would like gratefully thank you to the member of Takaguchi's group for their helping in experimental work.

I would say thank you to Dr. Hideaki Miyake for TEM measurement.

I would say thank you to Wataru Kurashige-sensei and Yuichi Negishi-sensei for Photo Luminescence (PL) intensity measurement.

Finally, I would like to express my deep gratitude to my parent and close family for all their encouragement and support during the last three years.

September, 2017

Kiki Kurniawan

List of Publications

Publication for this thesis

1. Incorporating a TiO_x Shell in Single-Walled Carbon Nanotube/Fullerodendron Coaxial Nanowires: Increasing the Photocatalytic Evolution of H₂ from Water under Irradiation with Visible Light
Kiki Kurniawan, Tomoyuki Tajima, Yosuke Kubo, Hideaki Miyake, Wataru Kurashige, Yuichi Negishi, Yutaka Takaguchi. *RSC Advances*, Vol.7, pp. 31767 - 31770 (2017).

Other papers

1. H₂-evolving SWCNT Photocatalysts for Effective Use of Solar Energy
Kiki Kurniawan, Noritake Murakami, Yuto Tango, Takumi Izawa, Kakeru Nishikawa, Ken Watanabe, Hideaki Miyake, Tomoyuki Tajima, Yutaka Takaguchi
NRS Conference Proceeding, In press (2017) (peer reviewed).